SEDIMENTOLOGY the journal of the International Association of Sedimentologists IAS

Sedimentology (2026) **73**, 2519–2547 doi: 10.1111/sed.70142

Petrology of modern river sands in China across tectonic, topographic and climatic gradients: Implications for sediment generation

SIYUAN FANG*, XING JIAN*, XIAOTIAN SHEN*, YUHAO CHEN*, LING WANG*,†, HANGHAI LIANG*, SHUO ZHANG*,‡ and HANJING FU*,§

**State Key Laboratory of Marine Environmental Science, College of Ocean and Earth Sciences, Xiamen University, Xiamen 361102, China (E-mail: xjian@xmu.edu.cn)*

†State Key Laboratory of Marine Geology, Tongji University, Shanghai 200092, China

‡Key Laboratory of Marine Geology and Environment, Institute of Oceanology, Chinese Academy of Sciences, Qingdao 266071, China

§Department of Ocean Engineering, Xiamen Ocean Vocational College, Xiamen 361102, China

Associate Editor: Xiumian Hu

ABSTRACT

Sandstone composition is widely used to infer tectonic setting, yet the combined effects of parent-rock lithology, climate and topography on sand composition and texture within sedimentary routing systems remain difficult to constrain. This study investigates modern river sands across diverse tectonic, topographic, climatic and bedrock-lithological settings in China, integrating quantitative compositional and textural data from 376 sediment samples. Our results show that sand composition is controlled primarily by parent-rock lithology rather than the tectonic setting of the bedrock. Sands derived from most lithologies broadly reflect their parent-rock characteristics, whereas carbonate and basaltic detritus exhibit more variable sedimentary behaviour owing to their higher susceptibility to weathering. Under strong physical erosion, rapid denudation and limited chemical weathering, carbonate and basaltic lithic fragments are preferentially preserved; conversely, they are readily decomposed or eliminated under more intense chemical weathering. Parent-rock lithology also governs the morphology of lithic fragments: low-grade metasedimentary rocks tend to produce elongated grains with high aspect ratios, whereas higher-grade metasedimentary or more resistant lithologies typically yield coarser and equant fragments. We contend that tectonic setting affects river sand composition mainly by establishing the regional parent-rock framework through ancient tectonic evolution and by shaping modern topography through neotectonic activity. Climatic influence on coarse-grained sediments is most clearly recorded by carbonate lithic fragments, which decrease systematically from arid to humid regions. Given the distinct source-to-sink behaviours of sands and muds, we recommend conducting integrated mineralogical, petrographic and geochemical analyses on both detrital fractions, jointly considering tectonic, topographic, lithological and climatic controls to better understand river sediment generation processes. These findings suggest that tectonic interpretations based solely on sandstone composition should be treated with caution and provide a quantitative framework for extending modern river sand datasets to deep-time sedimentary systems.

Keywords Fluvial sediments, provenance analysis, sand petrology, sedimentary recycling, tectonics, weathering.

INTRODUCTION

River sediments preserve critical information on source regions, erosion and weathering processes and transport pathways. Decoding this information helps to reveal the dominant controlling mechanisms of geological processes behind them (Arribas *et al.*, 2007; Mazumder, 2017; Augustsson, 2021). River sediments in different tectonic (e.g., convergent, collisional and extensional), geomorphic (e.g., alluvial fans and glacial landscapes) and climatic (e.g., cold desert climate and humid subtropical climate) environments generally exhibit diverse textural (e.g., grain size and shape) and compositional features (Johnsson, 1993). Coarse-grained fractions (sand- and gravel-sized) and fine-grained fractions (silt- and clay-sized) in river sediments are characterised by contrasting generation processes, transport mechanisms and geological significance. Sand-sized sediments (>63 μm) are composed predominantly of erosional residues from parent rocks, and their compositions can commonly be used to reflect provenance information (Caracciolo, 2020). In contrast, mud-sized sediments (<63 μm) are derived not only from inherited materials of parent rocks through physical erosion, but also from products of bedrock chemical weathering (i.e. newly formed materials). Their mineralogical and geochemical signatures are strongly controlled by climate, weathering intensity and transport history, making them more suitable for reconstructing source area weathering, palaeoclimatic and palaeoenvironmental conditions (von Eynatten *et al.*, 2012; Fu *et al.*, 2025). Consequently, most provenance studies have primarily focused on sand-sized detrital grains to achieve direct and reliable parent-rock reconstruction.

A variety of methods have been employed for sediment provenance analysis and parent-rock reconstruction that focus on sand-sized grains, including framework grain petrography and heavy mineral analysis, geochemical analysis of bulk sediments and detrital single-mineral analysis (e.g., *in situ* mineral chemistry, geochronology, thermochronology and isotopic analysis; Joshi *et al.*, 2021; Garzanti *et al.*, 2021a; Andersen *et al.*, 2022; Shen *et al.*, 2024; Ye *et al.*, 2024). Among these, framework petrography remains the most widely used and fundamental technique. Compared to heavy mineral or single-mineral analysis that focuses on minor components, framework petrography targets the major components of sand-sized sediments (Jian *et al.*, 2013; Gu *et al.*, 2025), offering a more comprehensive characterisation of detrital features. Unlike bulk geochemical analysis, it integrates both compositional and textural information (Borges & Huh, 2007; Le Pera *et al.*, 2023; Shen *et al.*, 2025), with its 'visible' microscopic analytical dimension, providing more intuitive and reliable interpretations of sediment provenance. This method, often based on the pioneering work of Dickinson and his subsequent modifications (Dickinson, 1970, 1985; Dickinson & Suczek, 1979; Weltje, 2006; Garzanti, 2016), allows for the discrimination of tectonic settings of sediment dispersal systems in both ancient and modern contexts. For instance, Dickinson (1985) classified tectonic settings into several categories, such as continental blocks, magmatic arcs and recycled orogens, by determining the relative proportions of framework grains in sands or sandstones. Garzanti (2019) further elaborated the relationships between framework grain compositions and tectonic settings and ultimately developed a classification system comprising 18 distinct fields.

Clarifying the relationships between sand/sandstone composition and tectonics is an important step in tracing sediment provenance and reconstructing tectonic settings. However, sediment generation processes and detrital compositions are also controlled by other critical factors, including the composition of a rock, which obviously determines parent-rock lithology, climate and topography in source-to-sink systems. These factors often interact in a coupled manner, producing complex effects on sediment products (Van de Kamp, 2010; Fu *et al.*, 2022; Demurtas *et al.*, 2024). Parent-rock lithology is the primary factor controlling sediment composition and texture. The mineral composition of a rock obviously determines the types and proportions of weathering residues and newly-formed products (Marques *et al.*, 2017; Babechuk & Fedo, 2023). Previous studies proposed the Sand Generation Index (SGI) to reflect the rock's potential to generate sand-sized detritus under specific climatic and topographic conditions (Kroonenberg, 1992; Arribas *et al.*, 2000; Garzanti *et al.*, 2013, 2018). Furthermore, different rocks have variable erodibility and thus determine sediment composition and fluxes (Moosdorf *et al.*, 2018; Liedel *et al.*, 2024). For river systems, the proportions of sedimentary bedrock in catchments determine the degree of sedimentary recycling (Zoleikhaei *et al.*, 2022; Liang & Yang, 2023).

Climate continuously modifies and filters sediment composition through its control of erosion, weathering, transport and deposition processes, thereby overprinting the original provenance information (Garzanti, 2019; Garzanti *et al.*, 2021b, 2021c). Generally, under cold or arid climates, physical processes dominate, allowing unstable minerals such as feldspar to be preserved (Van de Kamp, 2010; Garzanti *et al.*, 2023a). Consequently, sand compositions may more closely reflect the actual proportions of parent rocks. In warm and humid climates, intense chemical weathering preferentially breaks down unstable minerals, leading to the relative enrichment of stable components and potentially resulting in misinterpretation of provenance (Schneider *et al.*, 2016; He *et al.*, 2025). Climate not only controls weathering conditions and sediment generation in source areas but also influences sediment transport and sorting mechanisms. In arid climates, wind-dominated transport results in well-rounded and well-sorted aeolian sands (Dott Jr, 2003; Garzanti *et al.*, 2015; Chen *et al.*, 2022). In extremely cold climates, glacial transport leads to poorly sorted tillites characterised by significant angularity and a wide grain-size distribution (He *et al.*, 2022). Under monsoon climates, river systems exhibit seasonal hydrological cycles, commonly characterised by high-energy hydrodynamic events and enhanced erosion processes (Singh *et al.*, 2007; Garzanti *et al.*, 2008; Garzanti, 2017). Furthermore, the composition and textural distribution of detrital sediments are largely controlled by their 'production-transport' history, which is strongly influenced by the topographic settings of river systems. Steep terrain typically requires a lower discharge to reach the erosion threshold, resulting in a longer effective erosion duration, higher average erosion rates and better preservation of bedrock information (DiBiase & Whipple, 2011; Schneider *et al.*, 2016).

This study aims to establish a new framework to investigate variations in the composition and texture of modern river sands under contrasting tectonics, bedrock lithology, climate and topography conditions. China was selected as the study area due to its diverse and well-defined lithologies, complex tectonic framework, nearly complete spectrum of climate zones and full topographic gradient from high mountains to flat plains (Fu *et al.*, 2025). This diversity enables a comprehensive examination of varying provenance signals responding to the coupling among the above-mentioned multi-factors. We compiled sand framework petrographic data from 376 sediment samples across 85 catchments in most regions of China (Fig. 1A). The dataset includes 136 samples analysed by our research team at Xiamen University, providing coverage of representative catchments across major geomorphological units, climate zones and diverse bedrock lithologies. Different kinds of catchments in the southeast China coastal region were particularly focused on because the river bedrock lithologies are relatively well-defined, and this region is characterised by a warm and humid climate with seasonal precipitation and extreme rainfall events (Zhang *et al.*, 2009; Wang *et al.*, 2024). This region exhibits a relatively tectonically stable setting and moderate topographic relief without high mountainous terrain (Fig. 2; Jian *et al.*, 2020a; He *et al.*, 2020). Furthermore, shorter rivers with relatively homogeneous bedrock lithology were also investigated, allowing a more systematic discussion of lithological controls (Fig. 3).

GEOLOGICAL AND CLIMATIC SETTING

The southeast China coastal region

The studied river systems in the southeast China coastal region exhibit warm, humid and mild erosion conditions. These include three mesoscale mountainous rivers (the Minjiang, Jiulongjiang and Hanjiang Rivers) and five small mountainous rivers (the Zhangjiang, Jinjiang, Mulanxi, Jiaoxi and Tongshanxi Rivers). This region is located in the tectonically stable Cathaysia Block. All the studied mountainous rivers originate from the Wuyi–Yunkai Orogenic Belt and its southward extension, the Daiyun Mountains, except for the Zhangpu coastal rivers, which are sourced from hills within the county (Li *et al.*, 2025). These rivers primarily flow through terrains dominated by low to medium mountains and hills. The overall topography exhibits a step-like decline from the northwest to the southeast, with average elevations in the upstream areas mostly ranging from 200 to 500 m and some headwater regions reaching 1000 to 2000 m. In contrast, the average elevation of downstream and estuarine plains rapidly drops to approximately 10 to 50 m, forming a typical geomorphological pattern of mesoscale

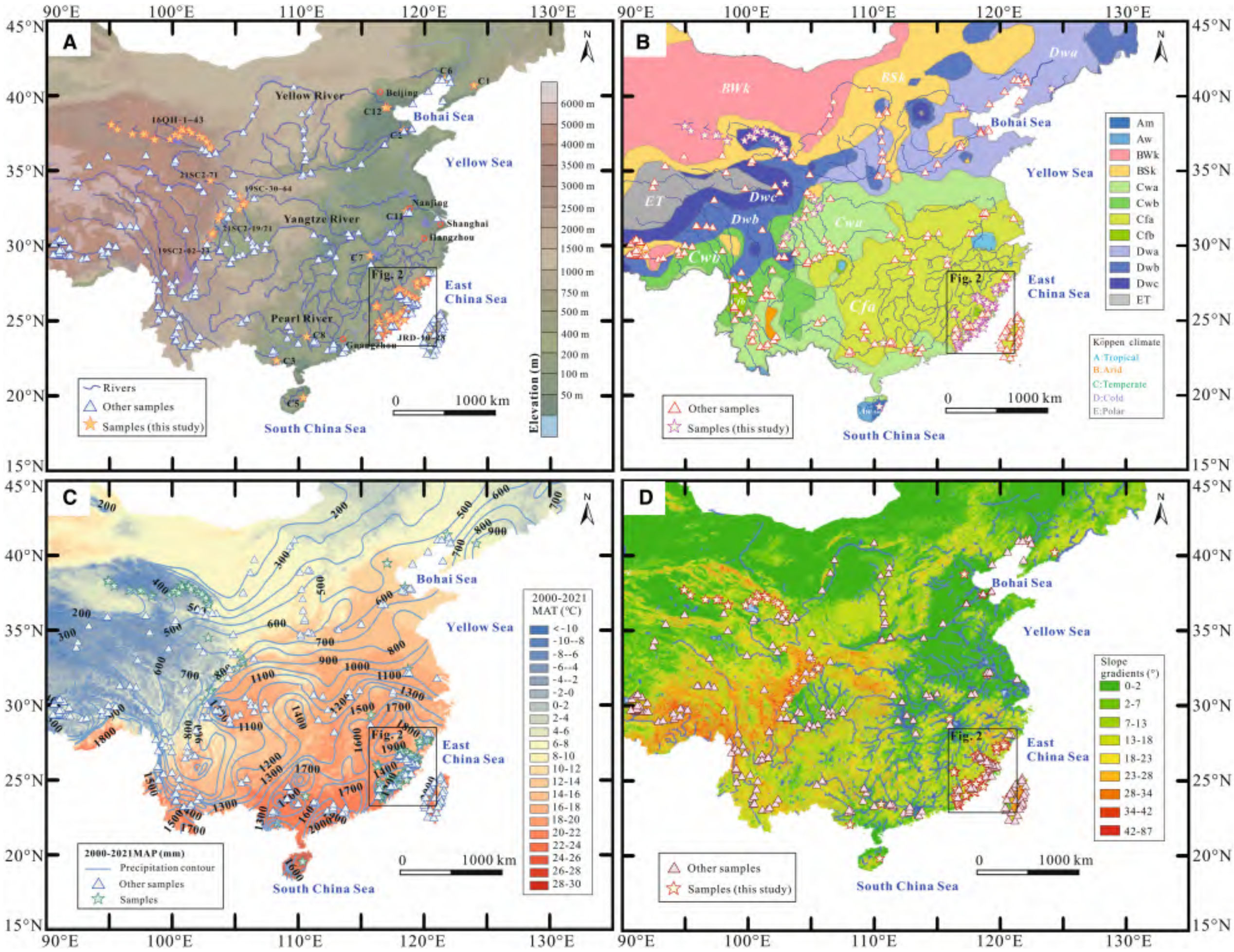

Fig. 1. Overview of the study area and sampling locations of modern river sands. Stars denote samples collected by this research team; triangles represent samples compiled from other studies, and blue curves indicate rivers). Climate types follow the Köppen classification: Am (Tropical monsoon), Aw (Tropical savanna), BSk (Cold steppe), BWk (Cold desert), Cfa (Humid subtropical), Cwa (Temperate with dry winter), Cwb (Subtropical highland), Dwa (Hot-summer humid continental), Dwb (Warm-summer humid continental) and ET (Tundra) (Zeroual *et al.*, 2019; Wu *et al.*, 2021). (A) Topography, river networks, sampling sites (this study and others) and major cities (red circles with black labels). (B) Köppen climate classification, river systems and sampling sites (this study and others). (C) Mean annual temperature and precipitation isopleths (2000 to 2021, dark blue lines) along with sampling sites (this study and others). (D) Slope gradients, river networks and sampling sites (this study and others) in the study area.

mountainous rivers (Chen, 2021; Wang *et al.*, 2024; Liu *et al.*, 2024; Table 1). The Cathaysia Block, in which the studied river basins are located, is composed mainly of Palaeozoic and Mesozoic granites, igneous rocks, Precambrian metamorphic basement and Mesozoic sedimentary rocks (Shen *et al.*, 2021). We also included four shorter rivers with relatively homogeneous bedrock lithology: the Hulouxi River in Jinjiang City, dominated by Holocene sediments; the Liufang River in Longyan City, dominated by sandstones; the Lianhuaxi River in Tong'an District, Xiamen City, dominated by granite; and the Zhangpu coastal rivers in Zhangzhou City, dominated by basalt-bearing sedimentary rocks (Figs 2 and 3). These river basins are affected by a subtropical monsoon climate characterised by warm and humid conditions and frequent typhoon events (Su *et al.*, 2017; He *et al.*, 2020; Garzanti *et al.*, 2021c), with a mean annual temperature (MAT) of 16 to 21°C and a mean annual precipitation (MAP) of 1300 to 1800 mm

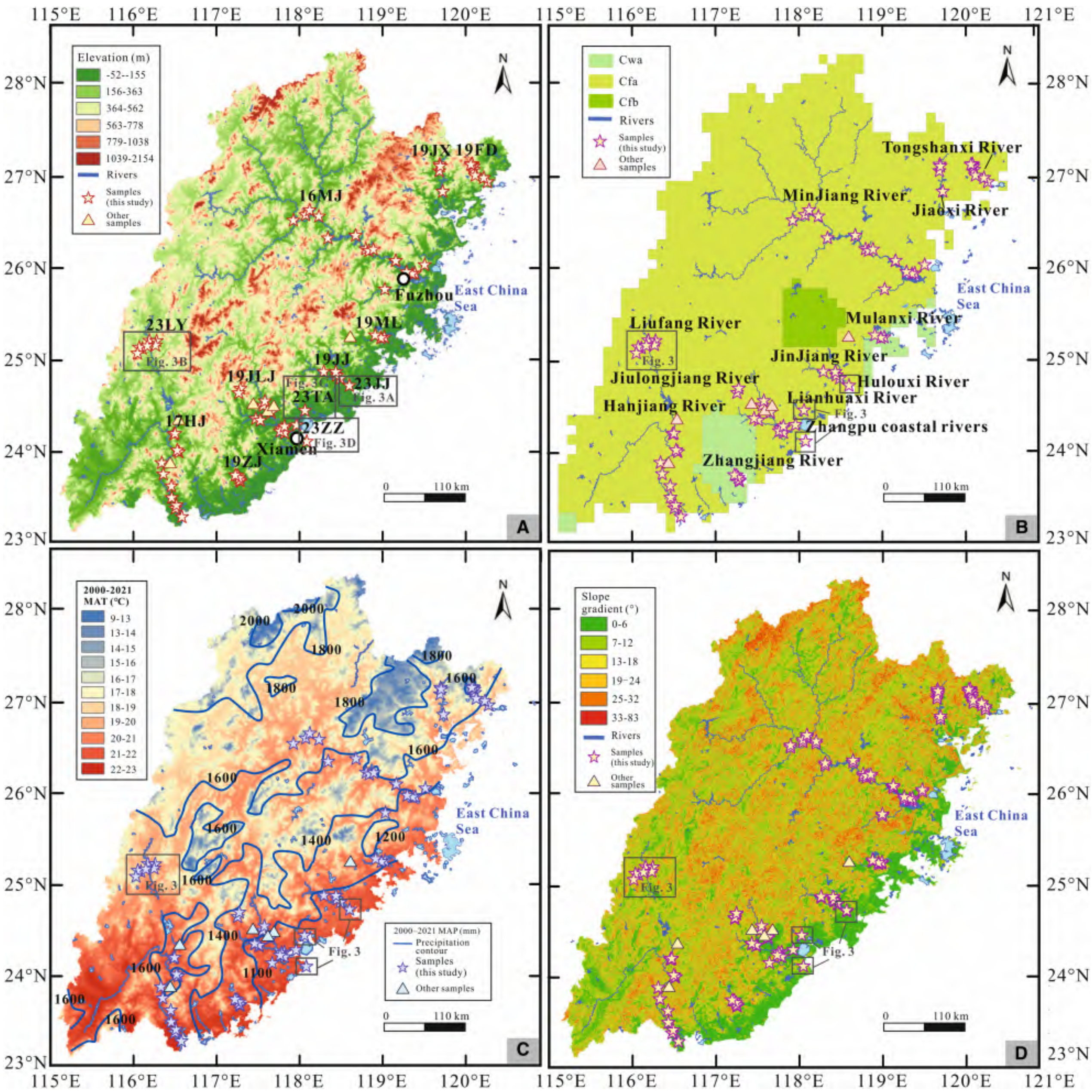

Fig. 2. Overview of the southeast China coastal region. Stars denote samples collected by this study, while triangles represent samples compiled from other studies; blue curves indicate rivers. (A) Topography, river networks and sampling locations (this study and others) in the southeast China coastal region. (B) Köppen climate classification, river systems and sampling locations (this study and others) in the southeast China coastal region. (C) Mean annual temperature and precipitation isopleths (2000 to 2021, dark blue lines) with sampling locations (this study and others) in the southeast China coastal region. (D) Slope gradients, river networks and sampling locations (this study and others) in the southeast China coastal region.

(Table 1; Fig. 2C). These rivers exhibit low erosion rates but rapid hydrological responses to seasonal precipitation (Su *et al.*, 2017; Jian *et al.*, 2020a, 2020b; Garzanti *et al.*, 2021a; Xu *et al.*, 2025).

The Taiwan region

We primarily focus on the Zhuoshui River in Taiwan, which originates from the main ridge of the Central Mountain Range at an elevation

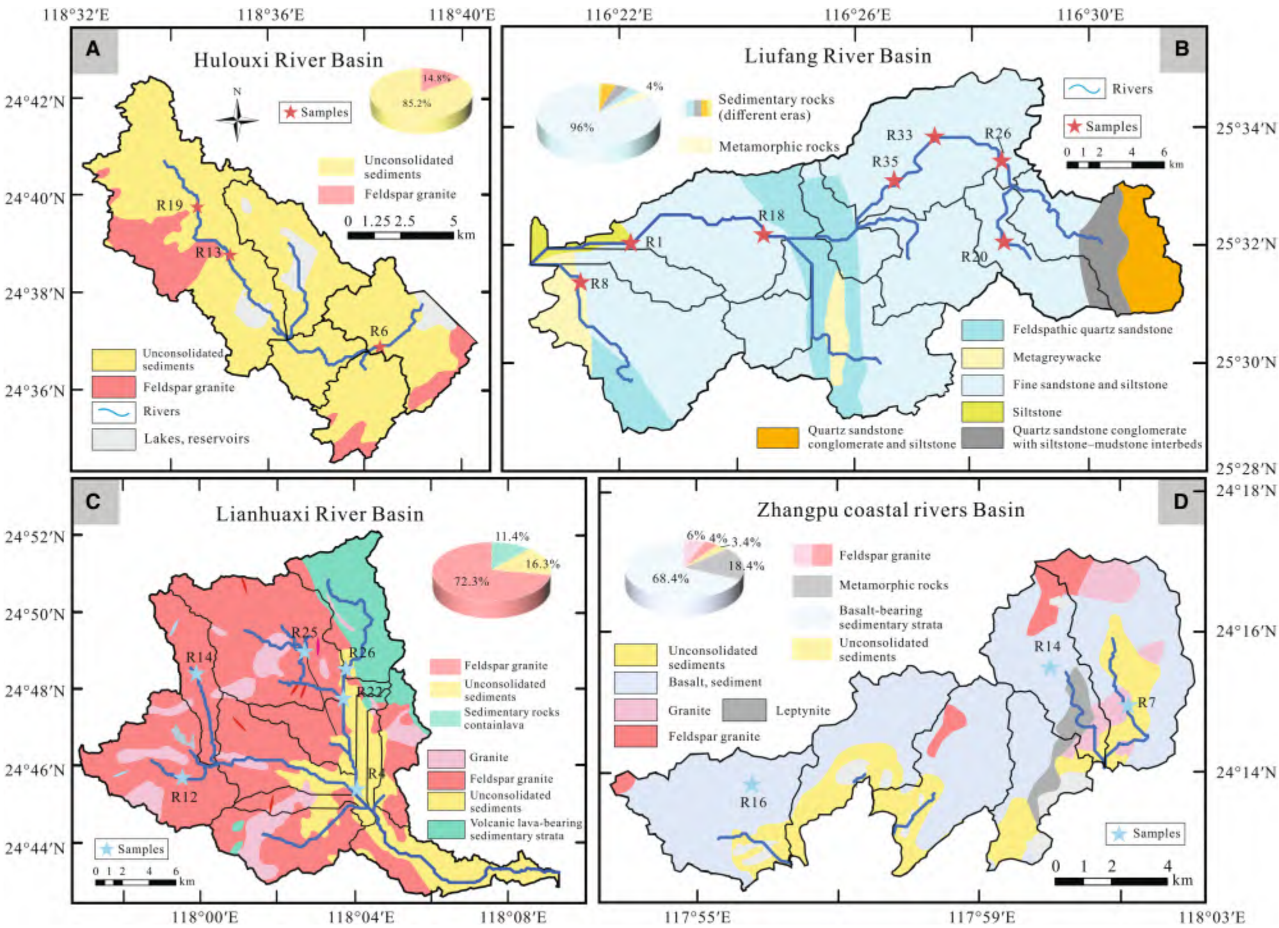

Fig. 3. Geological setting and sampling locations of small, lithologically homogeneous rivers in the southeast China coastal region. Circles indicate clay sampling sites, stars denote sediment sampling sites, blue curves represent rivers, light grey patches show lakes/reservoirs/ocean areas and pie charts illustrate lithological proportions within each catchment. (A) Hulouxi River basin, dominated by sedimentary sequences and feldspar granite. (B) Liufang River basin, exposing feldspathic quartz sandstones, metagraywacke, fine sandstones, siltstones, quartz sandstone-conglomerates (with siltstone-mudstone interbeds) and conglomerates. (C) Lianhuaxi River basin, containing granite, feldspar granite, sedimentary packages and volcanic lava. (D) Zhangpu coastal rivers basin, featuring sediment, granite, feldspar granite, basalt and leptynite.

exceeding 3400 m, in warm, humid and intense erosion conditions. The Central Mountain Range developed mainly in response to the oblique collision between the Luzon Island Arc and the Eurasian continental margin since ca 6 Ma, forming the modern high-relief topography of Taiwan (Lee *et al.*, 2006; Guan *et al.*, 2009). The Zhuoshui River flows westward from the Central Mountain Range through steep mountainous terrain, deep canyons and the western alluvial plain. The exposed bedrock in the basin is dominated by sedimentary and very low-grade metasedimentary rocks, including Eocene to Miocene slate and phyllite (Huang *et al.*, 2012a; Zhao *et al.*, 2017; Zhang *et al.*, 2022). The region is characterised by a subtropical monsoon climate with an average annual temperature of about 22.2°C and annual precipitation of up to 2232 mm, with frequent typhoons and concentrated heavy rainfall. These climatic conditions notably enhance surface runoff and erosional capacity (Table 1; Kao & Milliman, 2008; Garzanti & Resentini, 2016). Previous measurements indicate that this basin is one of the most severely eroded regions in the world, with erosion rates of 5 to 10 mm/a (Table 1; Dadson *et al.*, 2003; Bi *et al.*, 2015).

Table 1. Background characteristics of the studied river catchments.

Area	Rivers	Denudation rate (mm/a)	MAT (°C)	MAP (mm/a)	Sedimentary cycles	Bedrock lithology
The southeast China coastal region*	Minjiang	0.05	18.3	1687	2 to 3	Southeastern Part: Jurassic volcanic rocks → Cretaceous sedimentary rocks; Northwestern Part: Precambrian metasediments → Palaeozoic carbonates → Mesozoic igneous rocks
	Hanjiang		20.3	1518	2 to 3	
	Jiulongjiang		19.2	1392	1	
	Tongshanxi		17.9	1654	2 to 3	
	Jiaoxi		16.5	1790	2 to 3	
	Mulanxi		20.1	1301	1	
	Jinjiang		19.9	1312	1	
	Zhangjiang		20.9	1339	2 to 3	
The Taiwan region†	Zhuoshui	5.00	22.2	2232	≥3	Eocene-Miocene slate → phyllite
The Qinghai region‡	Shaliu	1.50	1.0	362	1	Precambrian metasediments → Palaeozoic sediments → Mesozoic igneous rocks
	Kaketuguole		1.0	200	2 to 3	Triassic magmatic rocks → Quaternary sediments → Silurian sedimentary rocks
	Bayin		4.0	182	2 to 3	Precambrian metasediments → Neoproterozoic-Early Palaeozoic metapelites → Late Permian gabbro → Cenozoic conglomerates/mudstones/gypsum
	Buha		1.0	362	2 to 3	Lower Silurian metasediments → Silurian granitoids → Middle-Late Triassic carbonates/clastics
	Datong		−4.1	524	≥3	Quaternary deposits → sedimentary rocks → metamorphic/volcanic rocks → local carbonates/intrusives
	Yuka		1.7	85	≥3	Caledonian granitoids → Hercynian-Indosinian intrusives → regional UHP metamorphics
	Haergai		1.0	362	2 to 3	Sinian metasediments → Cambrian-Ordovician marbles/metavolcanics → Silurian granite → Permian-Jurassic clastics
The Sichuan region§	Dachuan	0.72	16.0	1276	2 to 3	Proterozoic metavolcanics/metasediments → Devonian carbonates → Permian clastics → Sinian granite
	Xiaohezi			1200	2 to 3	Sinian dolomite → Silurian sedimentary rocks → Permian carbonates
	Qingjiang			1200	2 to 3	Triassic clastics/carbonates → Jurassic sandstones/conglomerates → Quaternary gravels
	Dongxi			1200	2 to 3	Paleoproterozoic mafic volcanics → Sinian tuff → Cambrian dolomite → Jurassic metavolcanics → Quaternary sediments
	Minjiang	0.26	12.1	600	≥3	Triassic sandstone → shale → gneiss
	Bailongjiang	0.26	8.0	750	≥3	Precambrian greenschists → Carboniferous sandstones → Jurassic sandstones
	Xiaofeishui	0.20	17.0	1100	2 to 3	Permian carbonates → Triassic sandstones → Jurassic mudstones

* Data from Peng (2019, 2020) and Xu *et al.* (2025). † Data from Bi *et al.* (2015) and Deng *et al.* (2020). ‡ Data from Mo *et al.* (2025), Ma *et al.* (2018), Hu *et al.* (2021), Wang *et al.* (2021b) and Li *et al.* (2014). § Data from Bai *et al.* (2025), Wang *et al.* (2022), Zhang *et al.* (2006) and Wang *et al.* (2021a).

The Qinghai region

The studied rivers in the Qinghai region are representative of cold, arid and intense erosion conditions. These are located in two tectonic domains: the Yuka River, Kaketuguole River and Bayin River on the eastern margin of the Qaidam Basin and the Datong River, Buha River, Shaliu River and Haergai River on the southern flank of the Qilian Mountains (Fig. 1A). All these rivers originate from high-altitude mountain areas with average elevations of approximately 5000 m (e.g., the Daken Daban Mountains and the Zongwulong Mountains; Jiang *et al.*, 2010; Yao *et al.*, 2012, 2013; Yang *et al.*, 2019). They traverse a dramatic topographic relief of 1000 to 2000 m before discharging into low-lying areas or terminal lakes (Xiang, 1982; Zhou *et al.*, 2000; Cui & Li, 2016). The bedrock of the river basins varies significantly: the eastern margin of the Qaidam Basin exposes strata from the Neoproterozoic to the Quaternary, including interbedded chlorite schist and marble, Ordovician metavolcanic rocks and Paleogene purplish-red mudrock (Fu *et al.*, 2014; Zhao *et al.*, 2017). The southern flank of the Qilian Mountains is dominated by the Precambrian basement of the Central Qilian Block and the South Qilian arc-accretion system, featuring Neoproterozoic to Early Palaeozoic plutonic rocks, Cambrian to Ordovician ophiolites and Triassic to Jurassic limestone and coal-bearing strata (Zhou *et al.*, 2000; Gehrels *et al.*, 2003; Tung *et al.*, 2013). The Qinghai region experiences a cold, arid continental plateau climate, with an annual average temperature not exceeding 4°C and annual precipitation ranging from 80 to 550 mm, concentrated mainly in summer. Topographic uplift results in local high-altitude areas receiving over 500 mm of precipitation (Table 1; Tang, 1985; Zhou *et al.*, 2000; Yao *et al.*, 2013). The eastern margin of the Qaidam Basin is dominated by aeolian processes, with a bedrock erosion rate of 0.05 to 0.4 mm/a (Rohrmann *et al.*, 2013; Table 1), while the Qilian Mountains region is in a state of uplift–erosion equilibrium, with an average erosion rate of approximately 1.5 mm/a (Hu *et al.*, 2021).

The Sichuan region

The targeted rivers in the Sichuan region develop under conditions of intense erosion and include the Minjiang (Sichuan), Bailongjiang, Qingjiang and Xiaohezi Rivers (Zhang *et al.*, 2011; Cook *et al.*, 2013; Tian *et al.*, 2013). These rivers originate from the Longmen Mountains and Minshan Mountains on the eastern margin of the Tibetan Plateau (Deng *et al.*, 1994; Zhao *et al.*, 1994a, 1994b; Searle, 2001) and flow through a zone of intense tectonic-topographic gradients along the eastern plateau margin, where tectonic activity is pronounced (Clark & Royden, 2000). The rivers originate from high-altitude mountainous areas at elevations of 5000 to 6000 m and descend sharply over a horizontal distance of approximately 50 to 60 km to the Sichuan Basin at about 600 m, resulting in dramatic topographic contrasts (Zhao *et al.*, 1994b; Searle, 2001). The bedrock lithology within the river basins is complex, centred on the Upper Proterozoic crystalline basement (metavolcanic and metasedimentary rocks of the Yangtze Craton), overlain by Palaeozoic passive continental margin metasedimentary sequences and thick Mesozoic foreland basin marine and clastic deposits, intruded by granite plutons of varying ages (Burchfiel *et al.*, 1995; Chengdu Institute of Geology and Mineral Resources, 2004). The region features diverse climate types, ranging from humid subtropical to alpine plateau climates, with temperatures of approximately 4 to 20°C and annual precipitation of 500 to 1200 mm. Precipitation is highly seasonal, with about 75% concentrated in summer (Table 1; New *et al.*, 2002; Zhang *et al.*, 2006). Driven by active tectonics and steep terrain, these rivers exhibit high erosion rates, averaging 0.75 mm/a (Table 1; Cook *et al.*, 2013; Tian *et al.*, 2013).

SAMPLING AND METHODS

Targeting these regions, a total of 136 river sand samples were collected. These samples include 89 samples from the Minjiang, Jiulongjiang, Hanjiang, Jinjiang, Zhangjiang, Tongshanxi, Jiaoxi, Mulanxi, Hulouxi, Lianhuaxi, Liufang and Zhangpu coastal rivers in the southeast China coastal region (2016 to 2023); 10 samples from the Minjiang (Sichuan), Bailongjiang, Qingjiang, Lujia, Dongxi, Dachuan, Xiaofeishui and Xiaohezi Rivers in the Sichuan region (2019 to 2021); 21 samples from the Buha River, Kaketuguole River, Bayin River, Yuka River, Shaliu River, Haergai River, Datong River, Saishikeguole River and Huaitoutala River in the Qinghai region (2016). Additionally, 11 samples were acquired from representative rivers across the country, including the Aihe River, Yellow River, Wanquan

River, Liaohe River and Pearl River. Furthermore, five samples from the top layers of a sedimentary core drilled in 2010 in the northern tidal flat of the Zhuoshui River estuary in Taiwan (Core JRD-N, elevation 7.94 m, coordinates 120°18.15′E, 23°54.17′N) (Zhang *et al.*, 2022) were selected for analysis as modern sands.

The collected river sand samples were wet sieved through a 500 μm stainless steel sieve to separate particles smaller than 500 μm, and the sieved fractions were then wet sieved through a 240-mesh nylon sieve to obtain 63 to 500 μm detrital components, which were subsequently dried. The separated fractions were then impregnated with Araldite resin and cut and polished into standard thin sections. The thin sections were then examined under a polarised-light microscope. Following the Gazzi–Dickinson methodology (Dickinson, 1985), more than 400 points per thin section were counted to determine the percentages of framework grains.

The equivalent spherical diameter (nominal diameter) was adopted to determine grain sizes, following the methodology outlined by Garzanti *et al.* (2008), based on transmitted-light photomicrographs of polished grain mounts. For individual grains, the maximum axis was recorded as the length (X), with the axis perpendicular to and bisecting the length designated as the width (Y). The third dimension (Z) was considered equivalent to the width. The grain size was subsequently derived from the cubic root of the product of these three orthogonal dimensions: $(X{\cdot}Y{\cdot}Z)^{1/3}$ (Lawrence *et al.*, 2011). To describe grain morphology, the aspect ratio was calculated as length/width. Roundness was evaluated according to the classic definition proposed by Wadell (1932), expressed as the mean curvature radius of all grain corners divided by the radius of the maximum inscribed circle within the grain outline. Roundness values were automatically computed using the MATLAB script developed by Resentini *et al.* (2018) and classified into three conventional categories: angular to subangular (0.1 to 0.4), subrounded to rounded (0.4 to 0.6) and well-rounded (0.6 to 1.0).

RESULTS

Composition of the analysed river sand samples

Representative photomicrographs of the analysed river sands from the four main study regions were selected and presented in Fig. 4, with the corresponding petrographic composition data provided in Table S1 in Appendix S1 and summarised in Table 2. More photomicrographs of the analysed samples are provided in Figs S1–S4 in Appendix S2.

Modern river sands from the southeast China coastal region mostly range from feldspatho-litho-quartzose to litho-feldspatho-quartzose, the average composition being feldspatho-litho-quartzose (Fig. 5A). Quartz is the most abundant component, followed by lithic fragments. These lithic fragments are dominated by sedimentary types, with subordinate metamorphic and magmatic lithic fragments, whereas carbonate lithic fragments are absent (Fig. S1F, Table 2). Although feldspar contents are locally high in some rivers, they are generally low overall and include both plagioclase and K-feldspar (Table 2).

Modern river sands from the Taiwan region are lithic-rich, with an average composition of quartzo-feldspatho-lithic (Fig. 5B). The sediments consist mainly of sedimentary lithic fragments, together with subordinate metamorphic and magmatic lithic fragments, whereas the remaining components are represented by approximately equal proportions of quartz and feldspar (Table 2).

In contrast, modern river sands from the Qinghai region range from quartzo-lithic to litho-quartzose, the average composition being quartzo-lithic (Fig. 5B). Lithic fragments are abundant (Table 2), dominated by metamorphic lithic fragments and carbonate lithic fragments (Figs S1A and B), with minor sedimentary and magmatic lithic fragments. Quartz is the second most abundant component. The feldspar content is the lowest on average among several study areas (Table 2).

River sands from the Sichuan region range widely from lithic to litho-feldspatho-quartzose, the average composition being feldspatho-quartzo-lithic (Fig. 5B). Lithic fragment content varies widely, dominated by carbonate lithic fragments and sedimentary lithic fragments, with minor metamorphic and magmatic lithic fragments (Table 2). Quartz ranks second on average, but in some rivers its content is extremely high, reaching up to 87.7% (Table 2).

Texture of the analysed river sand samples

Microscopic observations on thin sections of the full sample set show that the studied river sands

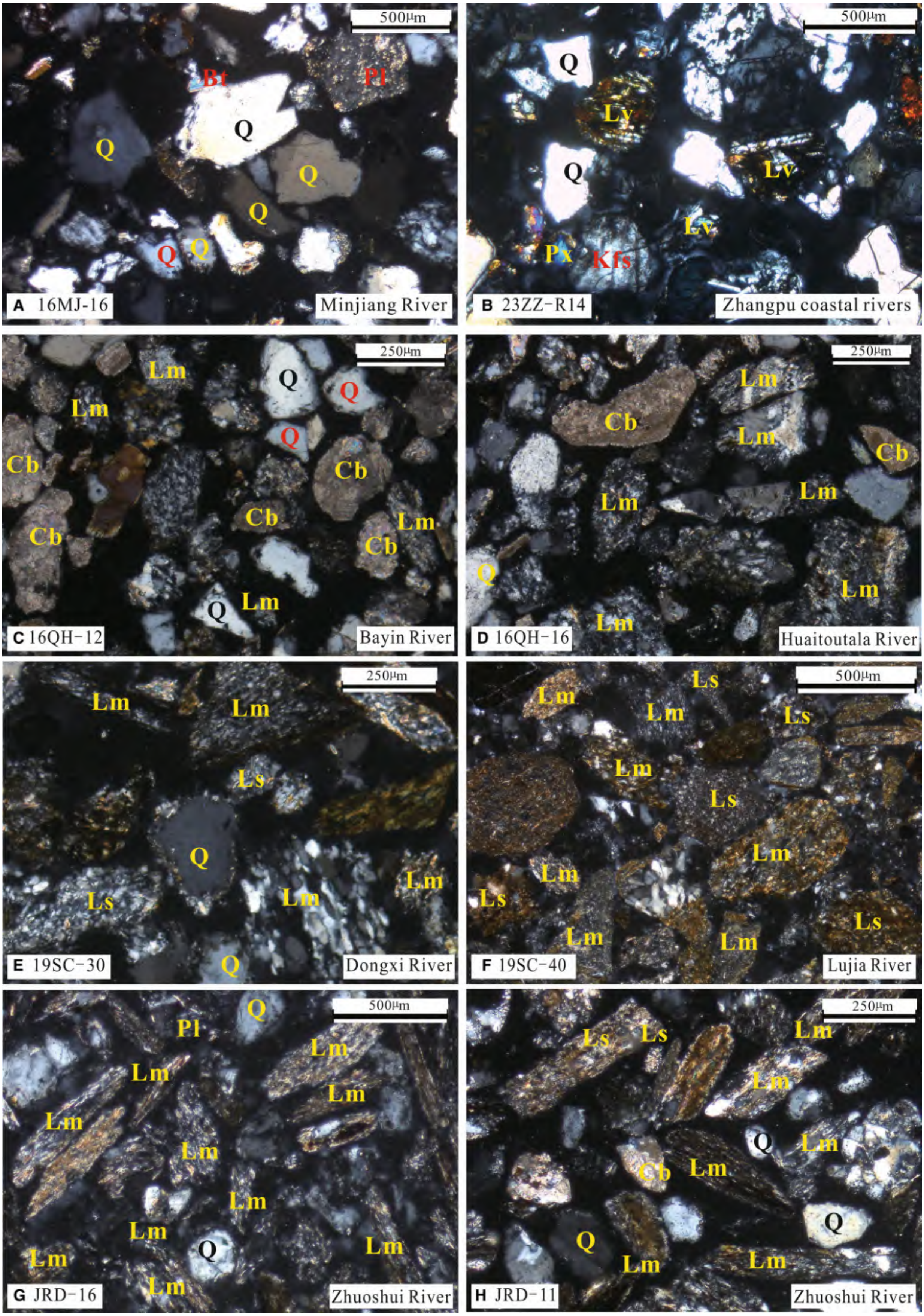

500μm
Bt
Pl
Q
A 16MJ-16
Minjiang River
500μm
Lv
Px
Kfs
B 23ZZ-R14
Zhangpu coastal rivers
250μm
Lm
Cb
C 16QH-12
Bayin River
250μm
D 16QH-16
Huaitoutala River
250μm
Ls
E 19SC-30
Dongxi River
500μm
F 19SC-40
Lujia River
500μm
G JRD-16
Zhuoshui River
250μm
H JRD-11
Zhuoshui River

Fig. 4. Representative photomicrographs of river sand samples from four study regions. (A) Sample 16MJ-16 from the Minjiang River, showing quartz, feldspar, biotite and sedimentary lithic fragments, with no carbonate lithic fragments observed. Grains are mostly granular to equant. (B) Sample 23ZZ-R14 from the Zhangpu coastal rivers, showing basaltic volcanic lithic fragments, quartz grains with embayed margins, pyroxene, plagioclase and K-feldspar. Grains are mostly granular. (C) Sample 16QH-12 from the Bayin River, showing abundant carbonate and metamorphic lithic fragments, commonly with short-columnar, equant or elliptical shapes. (D) Sample 16QH-16 from the Huaitoutala River, showing abundant metamorphic and carbonate lithic fragments, most of which are short-columnar to equant. (E) Sample 19SC-30 from the Dongxi River, showing sedimentary and metamorphic lithic fragments with variable shapes, ranging from subrounded to moderately elongated. (F) Sample 19SC-40 from the Lujia River, showing abundant sedimentary and metamorphic lithic fragments, commonly with subrounded, equant or slightly elongated shapes. (G) Sample JRD-16 from the Zhuoshui River, showing abundant elongated and foliated or striated metamorphic lithic fragments. (H) Sample JRD-11 from the Zhuoshui River, showing abundant elongated lithic fragments and foliated or striated metamorphic lithic fragments. Bt, biotite; Cb, carbonate lithic fragment; Kfs, K-feldspar; Lm, metamorphic lithic fragment; Ls, sedimentary lithic fragment; Lv, volcanic lithic fragment; Pl, plagioclase; Px, pyroxene; Q, quartz.

are texturally diverse. Detrital grains range from subangular to well-rounded, and lithic fragments display variable grain shapes and aspect ratios among different river systems. To quantify these textural variations, a total of 23 samples from 13 rivers across different regions were selected for quantitative textural analysis. Quantitative data on quartz roundness and the roundness and aspect ratios of lithic fragments from these samples are presented in Tables S3–S6 in Appendix S1 and Figs 6 and 7. Overall, the analysed sands exhibit grain shapes ranging from subangular to well-rounded, as illustrated in Fig. S2, whereas Fig. S4 shows the differences in aspect ratios among the studied samples. The proportions of well-rounded quartz grains were compared among river sands from the southeast China coastal study area, Qinghai region, Sichuan region and Taiwan region (Fig. 6), with detailed data summarised in Table 2. Additionally, the roundness and aspect ratio of lithic fragments from five rivers across three regions were compared (Figs S4 and S7), with detailed data summarised in Table 2.

Compilation of literature data on river sands from the study area

Previously published composition data from 240 samples in the study area were compiled. Sample locations are shown in Figs 1 and 2. The compiled petrographic data for all the river sediments show the following compositional ranges: quartz content varies from 1.1 to 88.4% (mean 49.9%), feldspar from 0 to 55.9% (mean 14.8%) and lithic fragments from 1.1 to 93.5% (mean 30.0%). The spatial heat maps integrating all the compositional data (after removing 16 samples from small, lithologically homogeneous rivers; a total of 360 samples remain, including 120 newly analysed samples and 240 previously published samples) indicate that quartz content is significantly higher in the subtropical monsoon region than in other climatic zones. In contrast, feldspar content is notably elevated in granitic source areas such as the southeast China coastal region. Lithic fragment contents are markedly higher in tectonically active regions (e.g., the Qilian Mountains) and in arid and cold climatic settings than in other environments (Fig. 8).

DISCUSSION

Influence of bedrock lithology on river sand composition

Our results show that catchment bedrock lithology is the principal factor determining river sand composition (Caracciolo *et al.*, 2012a, 2012b; Goswami & Deopa, 2018; Garzanti, 2019; Caracciolo, 2020). In the southeast China coastal region, sands from the Minjiang, Hanjiang and Jiulongjiang Rivers contain relatively high feldspar (average 22.30%) and quartz contents (average 60.11%) (Fig. 5A), reflecting the contributions of widespread granitoid parent rocks. The high mechanical strength and relatively low chemical weathering rates of this type of rock allow physical disaggregation to continuously supply sand-sized quartz and feldspar grains (Palomares & Arribas, 1993; Garzanti *et al.*, 2018), maintaining high detrital feldspar

Table 2. Petrographic composition and textural statistics of selected samples from the study area.

	River	Sample number	Quartz content (%)	Feldspar content (%)	Lithic fragment content (%)	Average modal composition	Well-rounded quartz grains (%)	Aspect ratio (lithic fragment)
The southeast China coastal region	Minjiang	16	40.4 to 74.5	14.2 to 42.6	2.0 to 21.5	$Q_{60}F_{24}L_{12}$	25.0	–
	Hanjiang	18	29.3 to 77.1	3.8 to 48.1	1.3 to 25.1	$Q_{60}F_{23}L_{13}$	40.0	–
	Tongshanxi	8	8.9 to 53.9	5.2 to 28.6	26.3 to 76.6	$Q_{38}F_{19}L_{42}$	33.3	–
	Jinjiang	5	49.5 to 68.1	10.4 to 19.4	21.5 to 34.1	$Q_{57}F_{15}L_{28}$	–	–
	Jiulongjiang	11	46.8 to 72.1	9.5 to 25.7	4.7 to 21.5	$Q_{60}F_{18}L_{14}$	23.3	–
	Jiaoxi	4	35.2 to 52.8	13.5 to 20.6	26.5 to 44.3	$Q_{44}F_{17}L_{37}$	–	–
	Mulanxi	3	53.4 to 61.1	12.8 to 18.3	18.8 to 26.4	$Q_{57}F_{16}L_{23}$	–	–
	Zhangjiang	5	46.5 to 61.4	8.9 to 15.7	29.1 to 37.8	$Q_{53}F_{12}L_{34}$	–	–
	Hulouxi	3	47.6 to 80.0	11.7 to 36.0	8.3 to 16.4	$Q_{62}F_{26}L_{12}$	–	–
	Liufang	7	65.6 to 88.4	0.0 to 2.0	9.7 to 33.0	$Q_{75}F_{1}L_{24}$	35.0	–
	Lianhuaxi	6	22.9 to 67.4	13.3 to 44.9	8.0 to 62.9	$Q_{51}F_{28}L_{21}$	23.3	–
	The Zhangpu coastal rivers	3	49.2 to 64.9	18.7 to 30.2	9.7 to 20.7	$Q_{59}F_{24}L_{16}$	–	–
The Taiwan region	Zhuoshui	5	4.1 to 16.2	12.2 to 24.7	62.9 to 79.8	$Q_{11}F_{17}L_{70}$	36.7	3.9
The Qinghai region	Buha	3	34.6 to 51.4	2.6 to 12.6	43.2 to 57.1	$Q_{42}F_{6}L_{50}$	26.7	–
	Shaliu						36.7	–
	Haergai						–	–
	Saishikeguole	10	8.5 to 43.9	2.3 to 10.6	44.1 to 80.0	$Q_{26}F_{7}L_{64}$	–	–
	Bayin						20.0	2.0
	Huaitoutala						–	2.0
	Yuka						36.7	–
	Kaketuguole						16.7	–
	Datong	10	27.6 to 68.6	2.8 to 9.9	19.2 to 63.7	$Q_{45}F_{6}L_{46}$	33.3	–
The Sichuan region	Lujia	4	3.0 to 87.7	3.8 to 8.2	8.1 to 78.1	$Q_{34}F_{7}L_{54}$	–	2.1
	Qingjiang						–	–
	Dongxi						16.7	2.4
	Datuanyu						–	–
	Xiaofeishui	3	23.5 to 26.2	13.4 to 30.8	38.1 to 47.6	$Q_{25}F_{20}L_{44}$	–	–
	Dachuan						33.3	–
	Xiaohezi						30.0	–
	Minjiang (Sichuan)	3	3.2 to 22.1	6.5 to 7.6	66.6 to 85.1	$Q_{10}F_{7}L_{77}$	–	–
	Bailongjiang						–	–

The dash '–' in the table shows unanalysed targets.

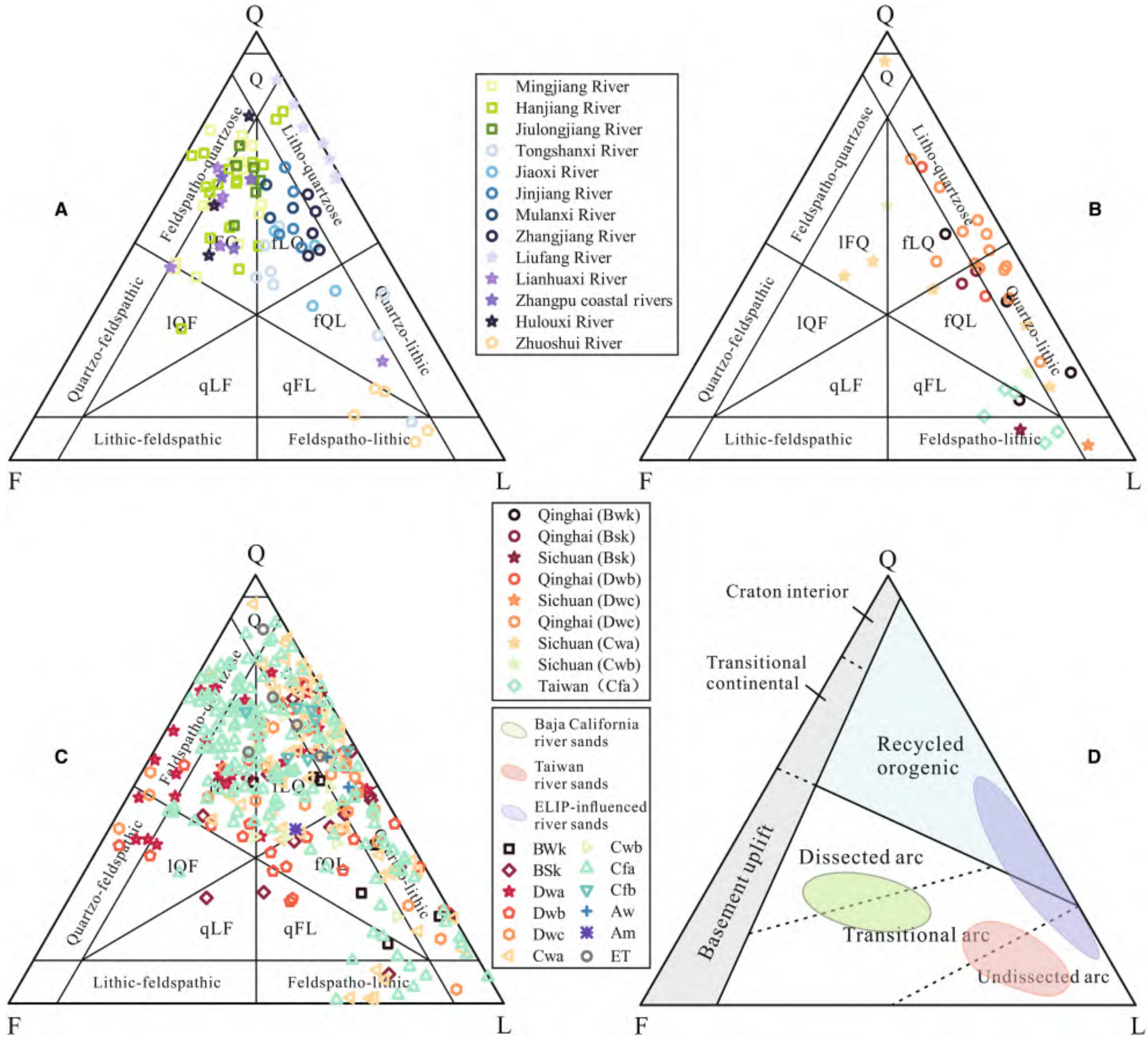

Fig. 5. Ternary diagrams of detrital modes for river sands in the study area. (A to C) Q-F-L diagrams for sandstone classification based on Garzanti (2019). In (A), samples are classified according to river type. Green series: large rivers in the southeast China coastal region; blue series: small mountainous rivers in the southeast China coastal region; purple series: shorter rivers with small, homogeneous lithology in the southeast China coastal region; orange series: rivers from Taiwan. In (B), rivers from Qinghai, Sichuan and Taiwan are classified and compared according to climate zone. Circles: rivers from Qinghai; stars: rivers from Sichuan; diamonds: rivers from Taiwan. Colours from dark red to cyan follow the climatic gradient from BWk to Cwa. In (C), all samples from the study area, including those analysed by our research group and previously published data compiled from Garzanti *et al.* (2018), Liang *et al.* (2022), Zhang *et al.* (2012), Borges *et al.* (2008), Borges & Huh (2007), Vezzoli *et al.* (2016), Garzanti *et al.* (2021b), Garzanti & Resentini (2016), Wang *et al.* (2013), Guo *et al.* (2020), Resentini *et al.* (2017), Nie *et al.* (2015) and Wang *et al.* (2019), are classified according to climate zone, with different colours and shapes representing different climate zones. (D) Q-F-L diagram for discriminating tectonic settings of provenance after Dickinson (1985). The green ellipse indicates the compositional field of river sands from the Baja California River, consistent with its actual tectonic setting. The pink ellipse indicates the compositional field of river sands from Taiwan, and the purple ellipse indicates the compositional field of ELIP-influenced river sands (ELIP = Emeishan Large Igneous Province, SW China). Note that these two compositional fields plot in areas inconsistent with their actual tectonic settings, reflecting the inherent limitations of the Dickinson tectonic discrimination diagram.

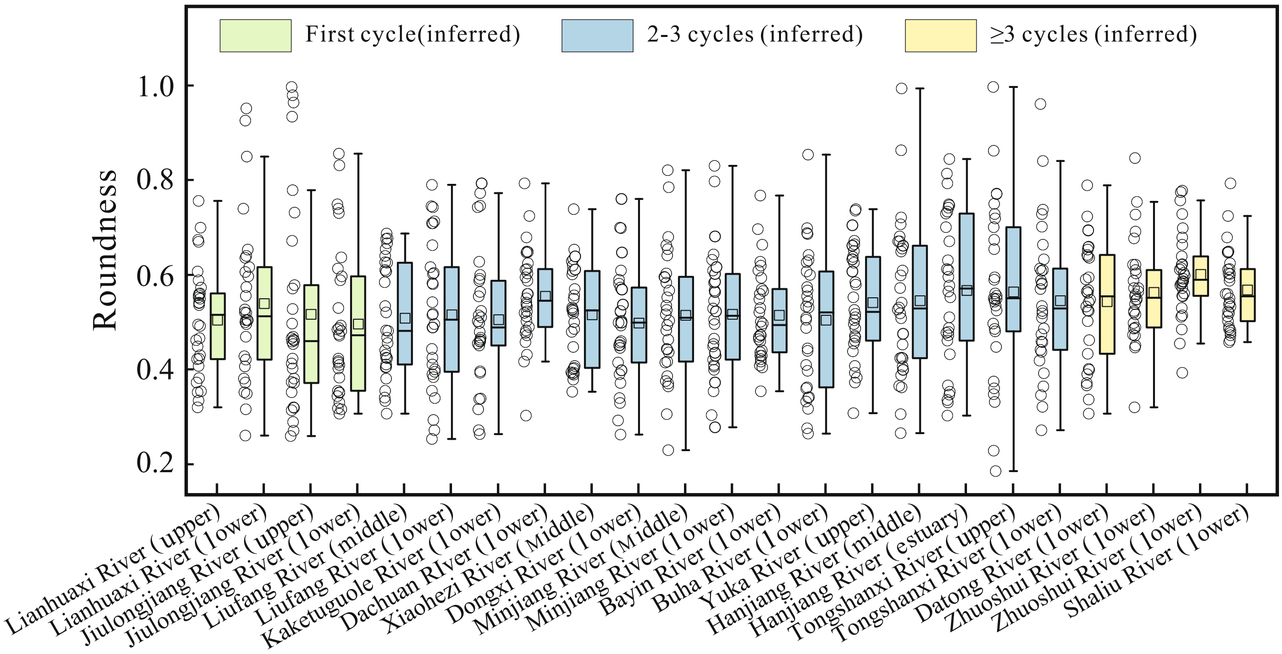

Fig. 6. Box plots of quartz-grain roundness classified by inferred sedimentary recycling cycles. Each box plot represents the distribution of roundness values for quartz grains in fluvial sediments from a single river. Box colours denote the inferred number of sedimentary cycles: blue represents the first cycle; green represents the 2 to 3 cycles; yellow represents the ≥3 cycles.

contents even under humid climatic conditions (Fig. 1B). Similar bedrock-lithology control is evident in river catchments in the Qinghai, Sichuan and Taiwan regions. Sands from the Bayin, Datong and Buha Rivers in the Qinghai region contain abundant metamorphic and carbonate lithic fragments, consistent with exposed metamorphic basement and Palaeozoic carbonate rocks in their catchments (Table 1; Figs S1A and S5B; Wei *et al.*, 2009; Zuza *et al.*, 2016; Feng *et al.*, 2024). Around the Sichuan Basin, rivers influenced by the steep Longmen Shan receive feldspar- and lithic-fragment-rich detritus from rapidly eroded sedimentary rocks, including sandstone, limestone and dolostone (Table 1; Fig. 5B). The Zhuoshui River Basin in Taiwan is dominated by low-grade metasedimentary and sedimentary rocks, including slate, shale, phyllite and schist, which readily disintegrate into lithic fragments (Garzanti *et al.*, 2023b). Our results are consistent with data reported by Garzanti & Resentini (2016), which showed that river sand composition and chemical weathering indices are controlled mainly by provenance rather than climate in Taiwan, as indicated by shale/slate-fragment-rich metasedimentary sands from the Backbone–Hsuehshan ranges and Slate Belt-derived lithic shale/slate sands in the upper Zhuoshui River.

Small, lithologically homogeneous rivers in the southeast China coastal region provide a more detailed perspective for investigating sediment generation mechanisms. The Liufang River catchment is mainly underlain by Jurassic micaceous quartz siltstone and shale of the Jurassic Zhangping Formation and quartz sandstone and quartz conglomerate of the Jurassic Lishan Formation (Fig. 2A; Zhang, 2024; Li *et al.*, 2025). These sands contain high quartz contents (average 74.82%), reflecting major contributions of quartz-rich parent rocks (Fig. S2D; Fig. 5C and D). By contrast, although sandstone bedrock occurs in the Tongshanxi River Basin, its lithic fragment-rich sands reflect dominant detrital supply of Mesozoic tuffaceous sandy conglomerate and fine sandstone, which account for up to 93% of exposed strata (Wang *et al.*, 2024). This can be explained as follows. Quartz sandstones weather mainly into quartz grains because of mechanically stable, quartz-cemented frameworks (Al-Harbi & Khan, 2005; Bassis *et al.*, 2016; Liu *et al.*, 2024), whereas tuffaceous sandstones,

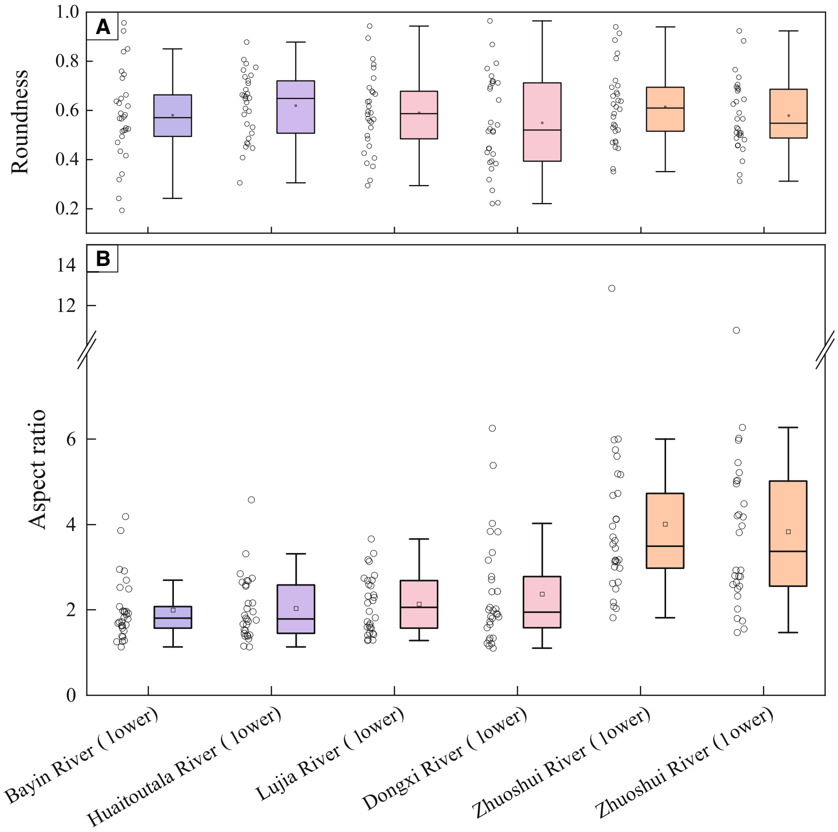

Fig. 7. Box plot comparison of textural characteristics of lithic fragments from Qinghai, Sichuan and Taiwan: (A) roundness comparison of detrital grains; (B) aspect ratio comparison of lithic fragments.

enriched in volcanic detritus and commonly less well-sorted or cemented, yield lithic-rich sands prone to fragmentation (Sun *et al.*, 2019; Le Pera & Morrone, 2020).

Among the small, lithologically homogeneous rivers in the southeast China coastal region, the Zhangpu coastal rivers are distinctive because they produce abundant volcaniclastic detritus. Their catchments include volcaniclastic-lacustrine-deltaic to intermontane-basin sedimentary sequences with interbedded basalt and clastic rocks (Fig. S3; Tang, 2022; Sun *et al.*, 2025). The Neogene Fotan Formation basalt accounts for about 13% of total stratigraphic thickness (Tang, 2022). Our results indicate that the sands therein contain 10% basaltic lithic fragments and 3% pyroxene on average (Fig. S3D; Table S1), indicating basaltic input. Other mafic-bedrock catchments differ: the basaltic lava-rich Uruguay River (SE South America) contains lower mafic magmatic lithic contents (Garzanti *et al.*, 2025), whereas the Hongshui River draining the Emeishan Large Igneous Province (SW China) contains notable mafic magmatic lithics that decrease downstream in the Pearl River (Garzanti *et al.*, 2021c). This difference may indicate that the generation and preservation of sand-sized detritus from basalt require more restrictive conditions. The small Zhangpu catchments, steep local relief, episodic high-intensity rainfall and short transport favour generation and preservation of fresh basaltic fragments. In contrast, in the Hongshui–Pearl River system, prolonged rainfall creates persistently humid conditions that, together with karst-related chemical weathering, reduce mafic lithic fragments downstream and the SGI for basalt progressively decreases from 1 in the Hongshui River to 0.5 at the Pearl River mouth (Palomares & Arribas, 1993; Garzanti *et al.*, 2021c).

Influence of bedrock lithology on river sand texture

The river sands examined in this study provide a representative example of how bedrock

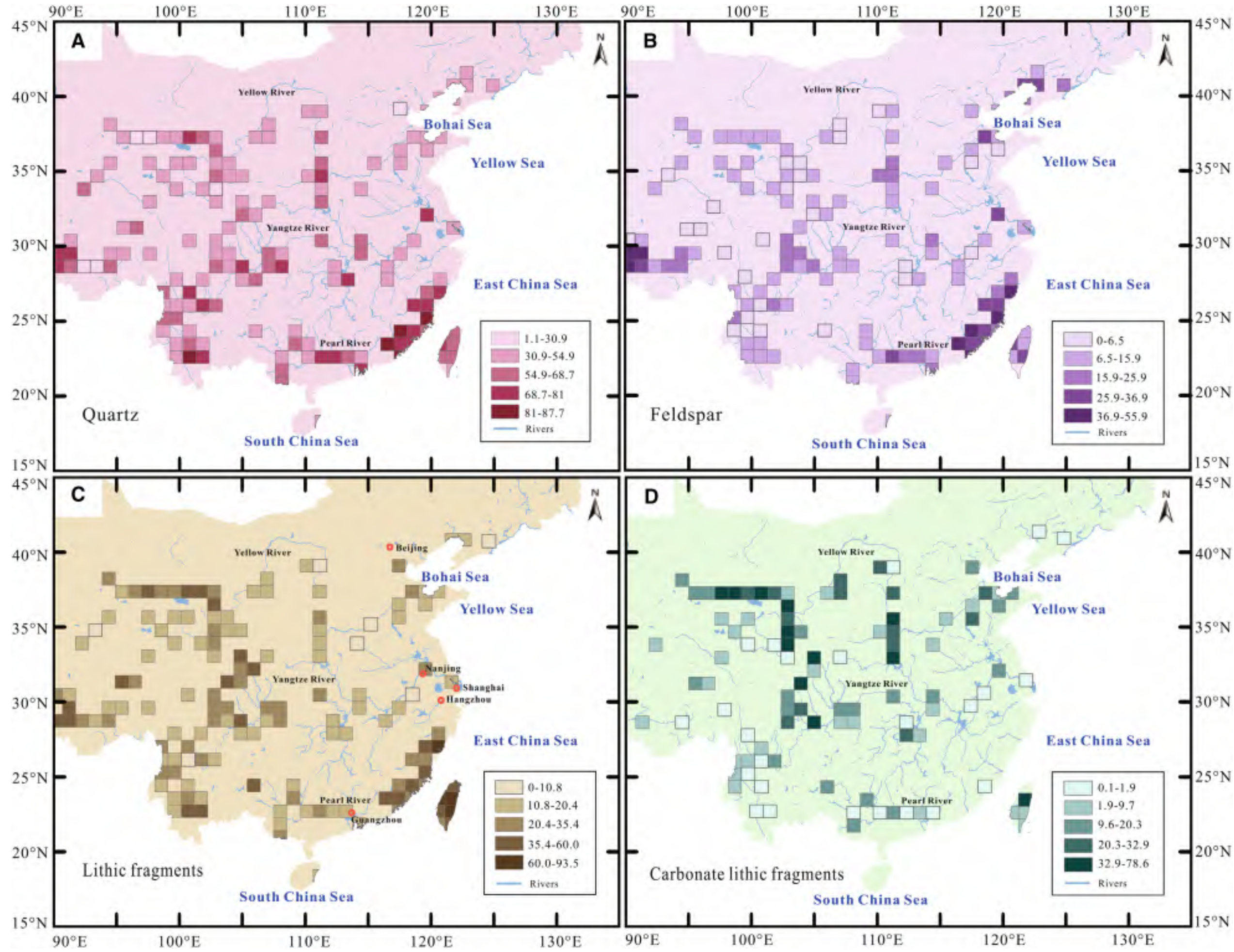

Fig. 8. Heat maps showing the contents of quartz, feldspar, lithic fragments and carbonate lithic fragments in the study area. Darker shades indicate higher particle content in the corresponding regions: (A) heat map of quartz content, with notably high values along the southeast China coastal region; (B) Heat map of feldspar content, showing a distribution pattern similar to that of quartz; (C) heat map of lithic fragment content (excluding carbonate lithic fragments), revealing relatively high abundances both in the southeast China coastal region and Qinghai region; (D) heat map of carbonate lithic fragments content, demonstrating elevated levels in Qinghai region, Sichuan region and parts of the Yellow River basin, while the southeast China coastal region is largely devoid of carbonate lithic fragments. Published data were compiled from Borges & Huh (2007), Borges *et al.* (2008), Zhang *et al.* (2012), Wang *et al.* (2013), Nie *et al.* (2015), Garzanti & Resentini (2016), Vezzoli *et al.* (2016), Resentini *et al.* (2017), Garzanti *et al.* (2018), Wang *et al.* (2019), Guo *et al.* (2020), Garzanti *et al.* (2021b) and Liang *et al.* (2022).

lithology controls sediment texture. In the samples subjected to textural analysis, quartz and feldspar grains show limited morphological variability, whereas lithic fragments display marked textural diversity. Results from rapidly eroding rivers in the Qinghai, Sichuan and Taiwan regions show that the aspect ratio of lithic fragments varies systematically with parent-rock lithology, although this signal may be modified by abrasion during transport (Krumbein, 1941). The Zhuoshui River Basin in Taiwan primarily exposes Eocene to Miocene slate and phyllite (Huang *et al.*, 2012b). Under the influence of metamorphism, foliation structures develop, aligning platy minerals and forming preferred fracture planes that cause the rock to split along foliation, producing naturally platy lithic fragments (Figs S4E and F; Powell, 1979; Garzanti & Vezzoli, 2003). In contrast, the Bayin River Basin in the Qinghai region exposes high-grade metamorphic gneiss (Yu *et al.*, 2017). Higher metasedimentary grade intensifies recrystallisation, coarsening mineral grains and yielding stubby-columnar or blocky lithic fragments (Fig. S4A; Drake, 1970). Lithic fragment shape is thought to be influenced not only by metasedimentary grade but also by erosion rate (Ayalew, 2009; Attal *et al.*, 2015). Although the Dongxi River in the Sichuan region also exposes low-grade metasedimentary rocks, the produced lithic fragments exhibit a lower aspect ratio compared to those from the Zhuoshui River (the Taiwan region; Fig. S4C–F, Table 2), likely due to relatively lower erosion rates in the Dongxi River Basin compared to the tectonically-active, high-precipitation Zhuoshui River Basin. A similar pattern occurs in rivers draining the Southern Alps, where medium- to low-grade metasedimentary rocks under rapid erosion also produce elongated lithic fragments (Garzanti *et al.*, 2006b).

Tectonic and erosion controls on river sand compositions

River sand composition has long been considered closely related to tectonic setting. Previous studies have widely compared sand modal compositions with ancient tectonic backgrounds. Dickinson (1985) developed tectonic discrimination diagrams based on sandstone framework-grain modes. For example, rivers in the Baja California Peninsula, Mexico, drain regions that form part of the Alisitos Arc. Their river sands are mainly classified as quartz–feldspar–lithic sandstones and lithic-feldspar-quartz sandstones, and thus they can be plotted within the magmatic-arc field in the Dickinson tectonic discrimination diagram (Le Pera *et al.*, 2023). This example indicates that, in some cases, the tectonic background recorded by river sands can show a close correspondence with the tectonic fields predicted by the Dickinson diagram. However, several cases in this study demonstrate that tectonic discrimination diagrams should not be applied uncritically. Taiwan is located in an arc–continent collision zone between the Eurasian Plate and the Philippine Sea Plate (Garzanti, 2016; Basu, 2017), but sands from most areas in Taiwan, such as those from the Zhuoshui River, overlap with the magmatic-arc field in the Dickinson diagram (Fig. 5D). This spurious tectonic signal mainly reflects the dominance of low-grade metasedimentary bedrock and the rapid supply of lithic fragments, rather than the actual tectonic setting of the basin. A similar problem occurs in catchments influenced by the Emeishan Large Igneous Province (SW China): contributions from mafic bedrock can shift sand composition toward the lithic-fragment end-member and cause samples to plot incorrectly in the magmatic-arc field rather than the transitional-continental field (Garzanti *et al.*, 2021c). As mentioned above, sand production processes in the mafic bedrock-rich catchments are quite variable and may confuse tectonic interpretations. These examples, together with previously reported failures of the Dickinson scheme in lithology-dominated systems (Garzanti, 2016; Caracciolo, 2020), emphasise the limitations of the Dickinson tectonic diagrams. We suggest that the Q-F-L fields should be interpreted as reflecting the combined effects of source lithology, climatic conditions, sedimentary processes and tectonic contexts, rather than the tectonic settings alone.

Tectonic influence on river sand composition can therefore be understood through two pathways. First, ancient tectonic-magmatic and tectonic-sedimentary evolution establishes the regional parent-rock framework. The Mesozoic Andean-type continental margin of southeast China, for instance, produced extensive granitic plutons that now supply quartz- and feldspar-rich detritus (Holloway, 1982; Charvet *et al.*, 1994; Li, 2000). Second, neotectonic activity, including mountain uplift, faulting and crustal shortening, controls modern topography and erosion patterns. Rapid uplift along the Longmen Shan fault zone, Cenozoic uplift of the Qilian Mountains and active collision in Taiwan generate steep relief, mass wasting, short sediment residence times and rapid delivery of feldspar and lithic fragments to rivers (Montgomery & Brandon, 2002; Bovet *et al.*, 2009; Garzanti & Resentini, 2016; Jiang *et al.*, 2020; Wang *et al.*, 2025).

Climate controls on river sand compositions

Temperature and precipitation, together with associated humidity, jointly control the intensity of chemical weathering on the Earth's surface (Van de Kamp, 2010). Box plots comparing the 376 river sand samples across different climatic zones show that quartz content generally increases from arid to humid regions, whereas feldspar and lithic fragment contents do not display clear climatic trends (Fig. 9A–C). The increase in quartz content is consistent with a

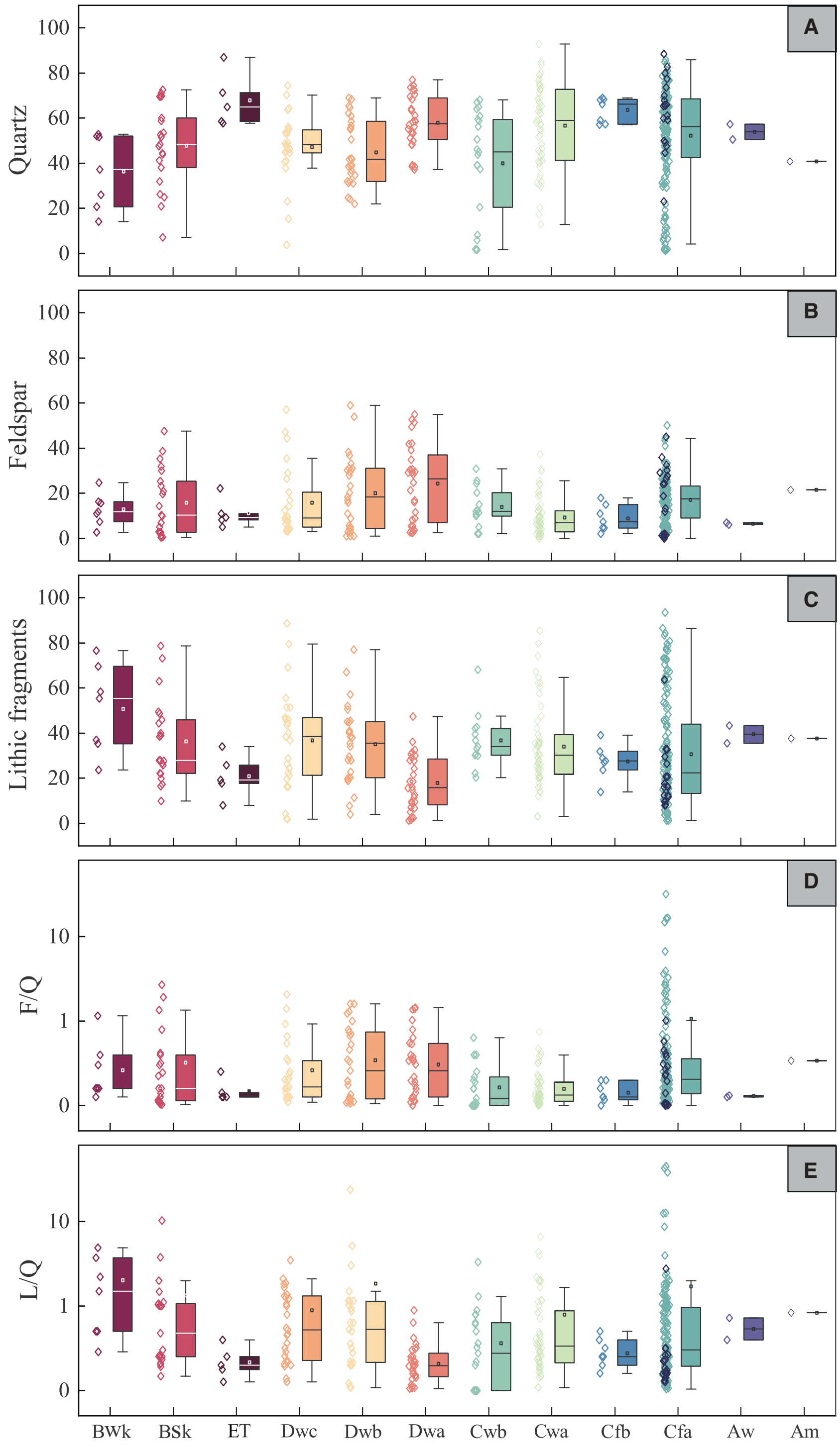

Fig. 9. Variations in detrital modes of river sands across climate zones. (A) Quartz (Q) content increases from arid to humid zones. (B) Feldspar (F) content shows no clear climatic trend. (C) Lithic fragment (L) content shows no clear climatic trend. (D) Feldspar/Quartz (F/Q) ratio. (E) Lithic fragment/Quartz (L/Q) ratio. Blue diamond symbols in the Cfa zone denote samples from short rivers in the southeast China coastal region. Published data were compiled from Borges & Huh (2007), Borges *et al.* (2008), Zhang *et al.* (2012), Wang *et al.* (2013), Nie *et al.* (2015), Garzanti & Resentini (2016), Vezzoli *et al.* (2016), Resentini *et al.* (2017), Garzanti *et al.* (2018), Wang *et al.* (2019), Guo *et al.* (2020), Garzanti *et al.* (2021b) and Liang *et al.* (2022).

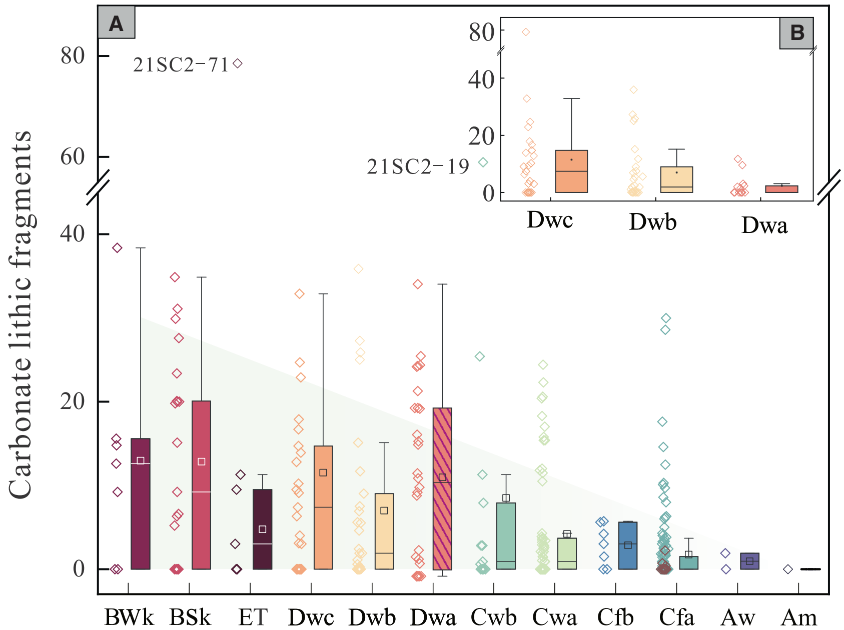

Fig. 10. Box plots comparing carbonate lithic fragment content in river sands across climate zones. (A) Overview of carbonate lithic fragment content variations. Content decreases markedly from arid to humid zones. Samples 21SC2-71 and 21SC2-19 are source area-controlled outliers with anomalously high carbonate supply. (B) The Dwa zone includes a high outlier due to exceptional carbonate contributions from parts of the Yellow River region; removal of this outlier clarifies the overall climatic trend. Red diamond symbols in the Cfa zone denote samples from short rivers in the southeast China coastal region.

fundamental weathering principle: intense chemical weathering in humid climates promotes the progressive decomposition and removal of unstable minerals, thereby resulting in the relative enrichment of more weathering-resistant quartz (Dinis *et al.*, 2017). Conversely, in arid and cold regions, weak chemical weathering combined with dominant physical weathering tends to favour the preservation of parent-rock signatures, including feldspar and lithic fragments, and consequently reduces the relative proportion of quartz in sand composition (Nesbitt & Young, 1996; Potter *et al.*, 2001; Zhang *et al.*, 2012). This means that those detrital components, which are strongly influenced by bedrock lithology and topography during sediment generation and routing, may obscure the climatic signal in coarse-grained sediment composition.

Among the detrital components, carbonate lithic fragments exhibit particularly high sensitivity to climate change, as the ratio of their chemical weathering rate to total denudation rate is much higher than that of most other rock types (Gaillardet *et al.*, 2019; Ott *et al.*, 2023; Figs 8 and 9). This climatic sensitivity is clearly reflected in the analysed river sands across various climatic zones (Fig. 10A), with carbonate lithic fragment content varying systematically from arid to humid settings. In arid regions, weak chemical weathering and dissolution allow carbonate lithic fragments to dominate the sediment composition where carbonate rocks are extensively exposed. The preservation of these soluble grains indicates high sediment transport rates and low weathering intensity (Abdullah *et al.*, 2023). A typical example is the Bayin River Basin (Qinghai region), characterised by a temperate continental climate with low annual precipitation (approximately 182 mm/a; Table 1), where river sands contain predominantly angular to subangular carbonate lithic fragments (Fig. S1A). In cold regions, the content of carbonate lithic fragments is comparatively lower (Figs 8D and 9B), as exemplified by the Jinsha River Basin (Borges *et al.*, 2008). This is probably due to the open valley topography and the gentle channel gradient (average slope 0.4‰), collectively prolonging sediment residence time and promoting gradual carbonate dissolution during sustained weathering (Liu *et al.*, 2023). In humid regions, by contrast, abundant rainfall drives near-complete carbonate dissolution (Fig. 10D; Das *et al.*, 2005; Singh *et al.*, 2006; Moon *et al.*, 2007). River sands from the Pearl River provide compelling evidence for this process: although carbonate rocks are widely exposed in the upper reaches of the Pearl River Basin (Lou *et al.*, 2014), carbonate lithic fragments are exceedingly scarce in the sediments delivered to the river mouth (Garzanti *et al.*, 2021b). This near-total absence reflects the combined effects of intense chemical weathering and karst processes: in the humid eastern part of the basin, well-developed tower karst landscapes facilitate the complete dissolution of carbonate grains during soil formation and sediment transport (Fig. 8D; Garzanti *et al.*, 2021c).

IMPLICATIONS

Implications for river sediment generation studies

This contribution mainly focuses on the controls on river sand composition and texture, while also recognising that river sands and muds (i.e., silt- and clay-sized sediments) generally have distinct source-to-sink behaviours in fluvial systems (Zhang *et al.*, 2021; Liang *et al.*, 2025). Previous studies have suggested that fine-grained sediments may provide unique insights into climatic and weathering dynamics. For example, clay-mineral assemblages (e.g., kaolinite/illite ratio) and the illite crystallinity index can distinguish intense weathering in humid tropics from weaker signals in arid or cold zones (Fig. 11D; Saha *et al.*, 2020; Wang *et al.*, 2024). Geochemical (e.g., CIA, Rb/Sr) and isotopic (e.g., $^{7}Li/^{6}Li$, $^{41}K/^{39}K$) proxies in muds help decipher catchment weathering history, denudation fluxes and transport dynamics (Jian *et al.*, 2020a, 2020b; Eyankware *et al.*, 2021; Oumar *et al.*, 2022). Similarly, the plagioclase/quartz ratio in silts effectively traces climatic conditions and weathering history (Fu *et al.*, 2025). However, as demonstrated in this study, the composition and texture of sand-sized river sediments are synthetically controlled by tectonic setting, bedrock characteristics and climate-modulated weathering and transport processes. Serving as the major weathering residues in fluvial systems, sand-sized sediments offer a distinct perspective for understanding sediment generation processes (Van de Kamp, 2010). The lower sensitivity of coarse detritus to direct climate signals may allow it to record the interplay between chemical weathering and physical erosion. A comparison of sand and mud signals could help disentangle tectonic and climatic controls. For example, if mud proxies vary while sand composition is stable, climate may dominate weathering; synchronous changes might reflect tectonic or geomorphic source alteration (Fig. 12; Yang *et al.*, 2004; Schneider *et al.*, 2016; Fu *et al.*, 2025).

Implications for deep-time sedimentary system studies

This study provides several important insights for deep-time sedimentology research. We originally attempted to explore whether textural parameters of detrital grains, such as quartz roundness, could be used to trace sedimentary recycling, a long-standing challenge in sedimentology, particularly in deep-time sedimentary systems. However, our preliminary data indicate that this relationship is more complex than initially expected. Our new data show that quartz roundness does not differ significantly between sediments derived from catchments with multiple recycling cycles and those from first-cycle detritus-dominated catchments (Table 1; Fig. S5). This observation is consistent with previous studies. For example, Garzanti (2017) showed that rounding of detrital grains during aqueous transport is generally slow; therefore, longer transport distances or prolonged transport histories do not necessarily result in greater roundness. In addition, chemical weathering may corrode quartz-grain margins, potentially leading to misinterpretation of quartz roundness as a purely mechanical rounding signal (Dott Jr, 2003). Further systematic studies incorporating larger datasets and more diverse depositional settings are therefore needed to better constrain the controls on detrital grain roundness and its applicability as a recycling proxy. Nevertheless, the sand textural features and their controlling mechanisms (such as the bedrock-lithological controls on sand shapes highlighted in this study), which were previously underestimated in sediment generation and sediment routing system studies, deserve more attention in both modern and deep-time system investigations. Furthermore, we propose

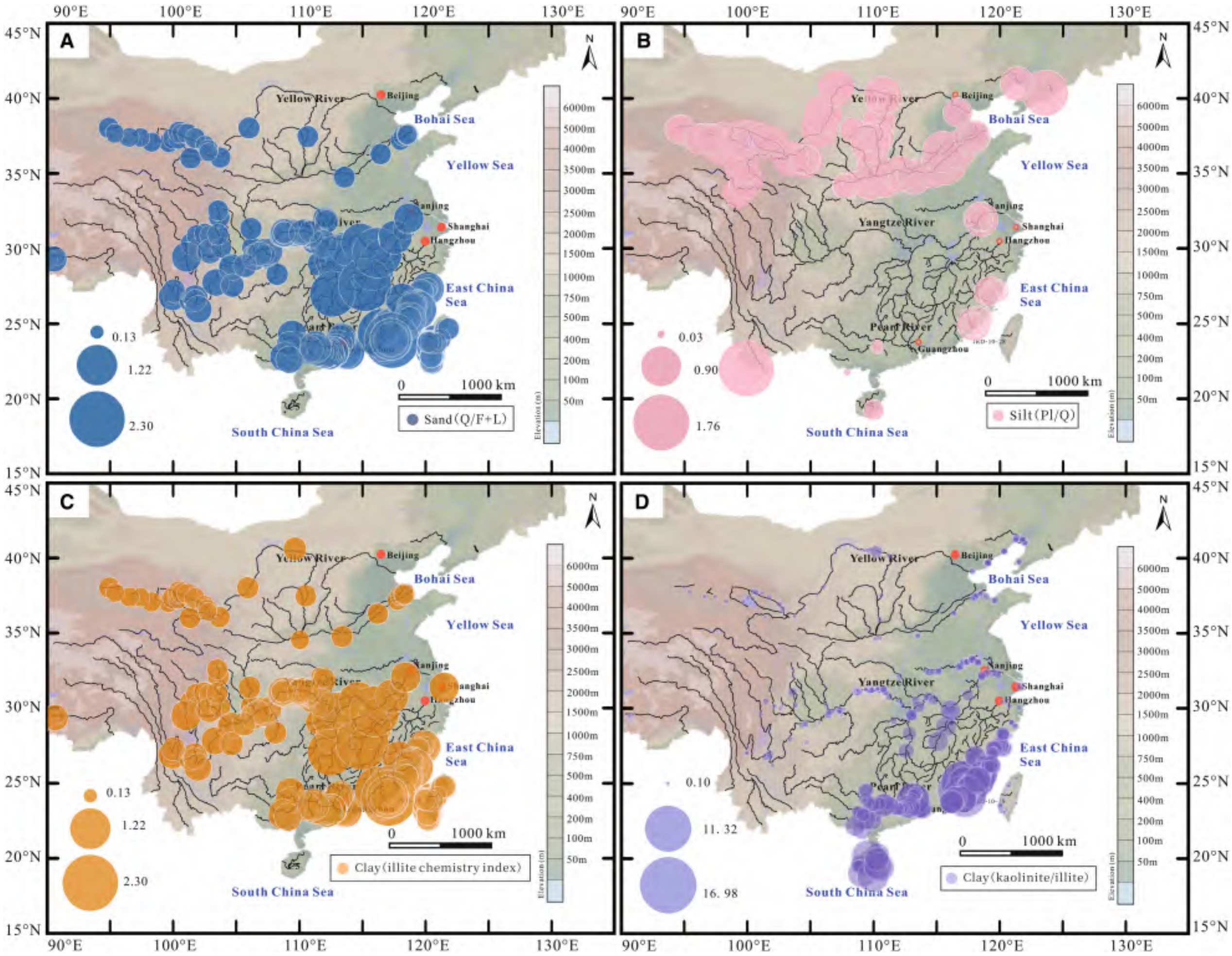

Fig. 11. Bubble map of weathering indices across China for sand, silt and clay fractions. (A) Sand-fraction index [Q/(F + L), blue bubble] reflecting the relative abundance of quartz compared with feldspar and lithic fragments; data are from analyses in this study and compiled sources. (B) Silt-fraction index (Pl/Q, red bubbles), indicating the ratio of plagioclase to quartz, data from Fu *et al.* (2025). (C) Clay-fraction index (Kaolinite/Illite, purple bubbles), reflecting silicate mineral weathering intensity, data from Wang *et al.* (2024). (D) Clay-fraction index [Illite Chemistry Index (ICI); orange bubbles], data from Wang *et al.* (2024).

that carbonate lithic fragments in sand-sized sediments are highly sensitive to climatic variation, and that their abundance may provide a semi-quantitative proxy for reconstructing palaeoclimate, particularly in sedimentary successions where carbonate components are well-preserved (Garzanti *et al.*, 2006a; Picard & McBride, 2007; Wu *et al.*, 2024).

CONCLUSIONS

Our comprehensive petrographic investigation of modern river sands, sampled across tectonic, topographic and climatic gradients, reveals that while sands from most lithologies faithfully preserve parent-rock signatures, those derived from easily weatherable rocks (e.g., carbonate rocks and basaltic rocks) constitute a distinct exception. Although mafic rocks are generally considered inefficient producers of sand-sized detritus under humid weathering conditions, the Zhangpu coastal rivers in SE China show that basalt-bearing bedrock can supply and preserve fresh mafic detritus under steep relief and episodic high-intensity rainfall conditions. Bedrock lithology also influences river sand texture. Low-grade metamorphic rocks with high erosion

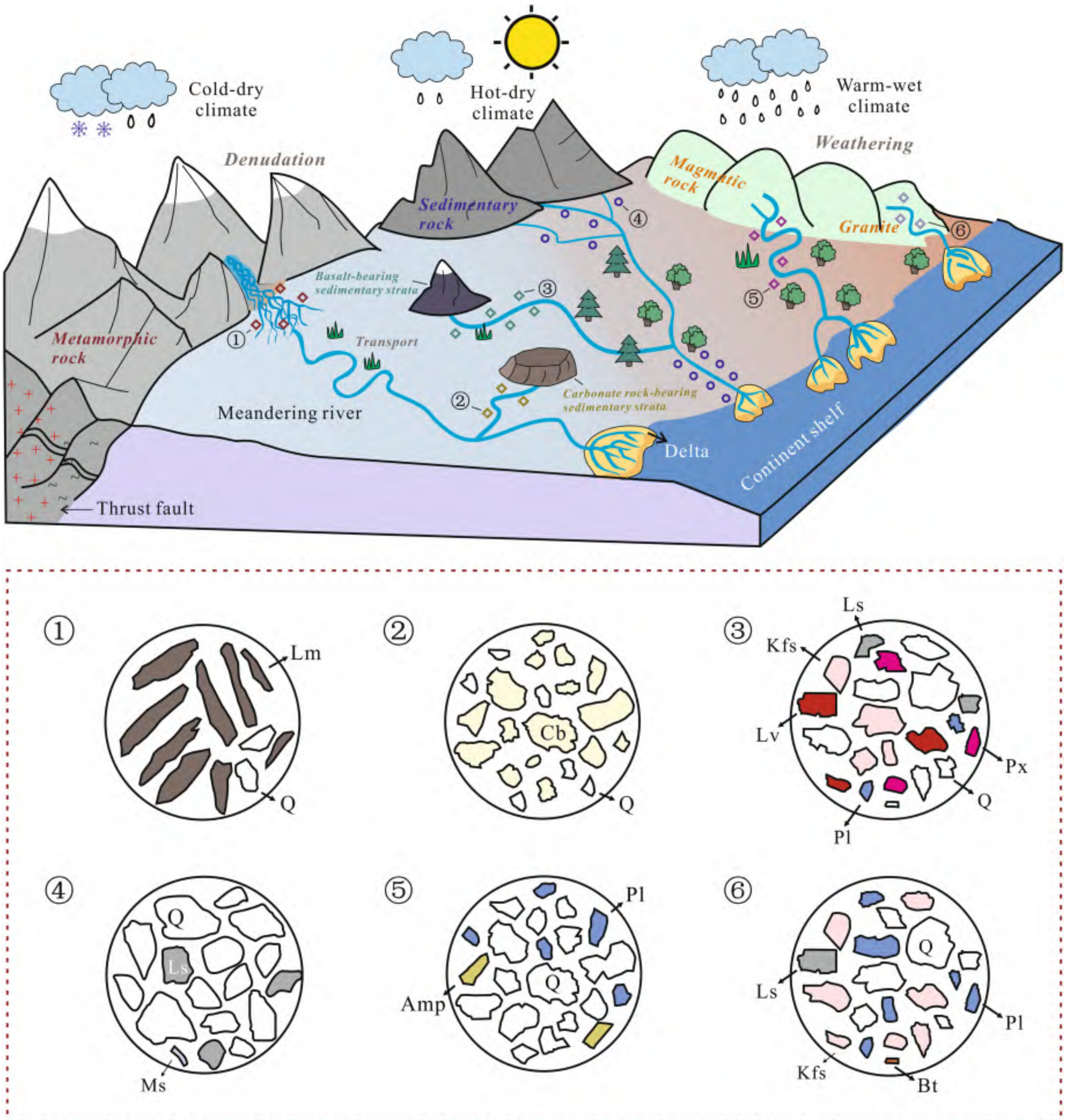

Fig. 12. Typical sediment compositions within a river system. The processes and factors in a sediment source-to-sink system include parent-rock lithology, climate, physical denudation, chemical weathering and sediment transport. Parent-rock lithology categories: volcanic-dominated, metamorphic-dominated, sedimentary-dominated, sedimentary strata containing basalt and sedimentary strata containing carbonate. The right side illustrates intense chemical weathering under a warm, humid climate (red background), while the left side illustrates weak chemical weathering under a cold, dry climate (blue background). Gentle hills on the right represent low erosion rates, whereas steep mountains on the left represent high erosion rates. Diamond symbols represent detrital material with low roundness; circular symbols represent detrital material with high roundness. (1) Sediment rich in blade-shaped lithic fragments, a product of shallow metamorphic parent-rock denudation; (2) sediment rich in carbonate lithic fragments, a product formed under low chemical weathering intensity; (3) sediment rich in mafic magmatic lithic fragments, a product of basalt denudation under high erosion rates; (4) sediment rich in high-roundness quartz, a product of a recycled (multicycle) geological background; (5) sediment containing a lot of quartz, a product formed under intense chemical weathering conditions; (6) sediment containing a granitic detrital assemblage, a product of a relatively homogeneous lithology. Amp, amphibole; Bt, biotite; Cb, carbonate lithic fragment; Kfs, K-feldspar; Lm, metamorphic lithic fragment; Ls, sedimentary lithic fragment; Ms, muscovite; Pl, plagioclase; Px, pyroxene; Q, quartz.

rates tend to produce elongated lithic fragments, whereas coarser and stubby fragments are more commonly derived from higher-grade or more resistant lithologies. Tectonic setting affects river sand composition mainly by establishing the regional parent-rock framework through ancient tectono-magmatic and tectono-sedimentary evolution, and by shaping modern topography and erosion patterns through neotectonic activity. Accordingly, active uplift and steep topography promote intense physical erosion and generate sands rich in lithic fragments and feldspar, whereas tectonically stable regions with gentle slopes tend to yield relatively quartz-rich sands. Climate exerts a secondary but important influence on sand composition by modifying the preservation of unstable components. Carbonate lithic fragments are particularly sensitive to climatic variation, and well-preserved carbonate-lithic-fragment-bearing clastic sequences may therefore be used to help reconstruct palaeoclimate. Together, these results highlight the primary role of bedrock lithology in controlling river sand composition and texture and provide new insights into sediment generation in both modern and deep-time sedimentary systems.

ACKNOWLEDGEMENTS

This research was supported by the National Natural Science Foundation of China (Nos. 42476051, 41806052) and the Natural Science Foundation of Xiamen, China (No. 3502Z20227006). We thank previous Xiamen University students Shuhuai Ye, Haowei Mei, Dongming Hong and Xuan Hu for their assistance in sample collection, laboratory analysis and theoretical discussions.

DECLARATION OF COMPETING INTEREST

The authors declare that they have no known competing financial interests or personal relationships that could have appeared to influence the work reported in this paper.

DATA AVAILABILITY STATEMENT

The data supporting the findings of this study (including Appendices S1 and S2) have been made publicly available on the Open Science Framework (OSF) platform at: https://osf.io/eruf9/overview.

REFERENCES

Abdullah, G.M., **El Aal, A.A.**, **Radwan, A.E.**, **Qadri, T.** and **Aly, N.** (2023) The influence of carbonate textures and rock composition on durability cycles and geomechanical aspects of carbonate rocks. *Acta Geotech.*, **18**, 105–125.

Al-Harbi, O.A. and **Khan, M.M.** (2005) Mineralogy and geochemistry of Unayzah Formation, Central Saudi Arabia: implications for provenance interpretation. *J. King Saud Univ.*, **18**, 35–49.

Andersen, T., **van Niekerk, H.** and **Elburg, M.A.** (2022) Detrital zircon in an active sedimentary recycling system: challenging the 'source-to-sink' approach to zircon-based provenance analysis. *Sedimentology*, **69**, 2436–2462.

Arribas, J., **Critelli, S.**, **Le Pera, E.** and **Tortosa, A.** (2000) Composition of modern stream sand derived from a mixture of sedimentary and metamorphic source rocks (Henares River, Central Spain). *Sed. Geol.*, **133**, 27–48.

Arribas, J., **Critelli, S.** and **Johnsson, M.J.** (Eds.) (2007) *Sedimentary Provenance and Petrogenesis: Perspectives from Petrography and Geochemistry*, Vol. **420**. Geological Society of America, Boulder.

Attal, M., **Mudd, S.M.**, **Hurst, M.D.**, **Weinman, B.**, **Yoo, K.** and **Naylor, M.** (2015) Impact of change in erosion rate and landscape steepness on hillslope and fluvial sediments grain size in the Feather River basin (Sierra Nevada, California). *Earth Surf. Dyn.*, **3**, 201–222.

Augustsson, C. (2021) Influencing factors on petrography interpretations in provenance research—a case-study review. *Geosciences*, **11**, 205.

Ayalew, T. (2009) Origin, texture, and classification of metamorphic rocks. *Geology*, **II**, 119.

Babechuk, M.G. and **Fedo, C.M.** (2023) Analysis of chemical weathering trends across three compositional dimensions: applications to modern and ancient mafic-rock weathering profiles. *Can. J. Earth Sci.*, **60**, 839–864.

Bai, L., **Liu, T.**, **Sha, A.** and **Li, D.** (2025) The spatiotemporal fluctuations of extreme rainfall and their potential influencing factors in Sichuan Province, China, from 1970 to 2022. *Remote Sens.*, **17**, 883.

Bassis, A., **Hinderer, M.** and **Meinhold, G.** (2016) Petrography and geochemistry of Palaeozoic quartz-rich sandstones from Saudi Arabia: implications for provenance and chemostratigraphy. *Arab. J. Geosci.*, **9**, 400.

Basu, A. (2017) Evolution of siliciclastic provenance inquiries: a critical appraisal. In: *Sediment Provenance, Influences on Compositional Change from Source to Sink* (Ed Mazumder, R.), Vol. **2**, pp. 5–23. Elsevier, Amsterdam, The Netherlands.

Bi, L., **Yang, S.**, **Li, C.**, **Guo, Y.**, **Wang, Q.**, **Liu, J.T.** and **Yin, P.** (2015) Geochemistry of river-borne clays entering the East China Sea indicates two contrasting types of weathering and sediment transport processes. *Geochem. Geophys. Geosyst.*, **16**, 3034–3052.

Borges, J. and **Huh, Y.** (2007) Petrography and chemistry of the bed sediments of the Red River in China and Vietnam: provenance and chemical weathering. *Sed. Geol.*, **194**, 155–168.

Borges, J.B., **Huh, Y.**, **Moon, S.** and **Noh, H.** (2008) Provenance and weathering control on river bed sediments of the eastern Tibetan Plateau and the Russian Far East. *Chem. Geol.*, **254**, 52–72.

Bovet, P.M., **Ritts, B.D.**, **Gehrels, G.**, **Abbink, A.O.**, **Darby, B.** and **Hourigan, J.** (2009) Evidence of Miocene crustal shortening in the north Qilian Shan from Cenozoic stratigraphy of the western Hexi Corridor, Gansu Province, China. *Am. J. Sci.*, **309**, 290–329.

Burchfiel, B.C., **Zhiliang, C.**, **Yupinc, L.** and **Royden, L.** (1995) Tectonics of the Longmen Shan and adjacent regions, central China. *Int. Geol. Rev.*, **37**, 661–735.

Caracciolo, L. (2020) Sediment generation and sediment routing systems from a quantitative provenance analysis perspective: review, application and future development. *Earth-Sci. Rev.*, **209**, 103226.

Caracciolo, L., **Tolosana-Delgado, R.**, **Le Pera, E.**, **von Eynatten, H.**, **Arribas, J.** and **Tarquini, S.** (2012a) Influence of granitoid textural parameters on sediment composition: implications for sediment generation. *Sed. Geol.*, **280**, 93–107.

Caracciolo, L., **von Eynatten, H.**, **Tolosana-Delgado, R.**, **Critelli, S.**, **Manetti, P.** and **Marchev, P.** (2012b) Petrological, geochemical, and statistical analysis of Eocene-Oligocene sandstones of the Western Thrace Basin, Greece and Bulgaria. *J. Sed. Res.*, **82**, 482–498.

Charvet, J., **Lapierre, H.** and **Yu, Y.** (1994) Geodynamic significance of the Mesozoic volcanism of southeastern China. *J. SE Asian Earth Sci.*, **9**, 387–396.

Chen, J. (2021) Engineering investigation analysis of western Fujian karst area focusing on rock, soil, and water. *Eng. Constr. Design*, **12**, 25–27.

Chen, B., **Yang, X.**, **Jiang, Q.**, **Liang, P.**, **Mackenzie, L.L.** and **Zhou, Y.** (2022) Geochemistry of aeolian sand in the Taklamakan Desert and Horqin Sandy Land, northern China: implications for weathering, recycling, and provenance. *Catena*, **208**, 105769.

Chengdu Institute of Geology and Mineral Resources (2004) *Geological Map of the Qinghai–Xizang (Tibet) Plateau and Adjacent Areas*. Geological Publishing House, Beijing.

Clark, M.K. and **Royden, L.H.** (2000) Topographic ooze: building the eastern margin of Tibet by lower crustal flow. *Geology*, **28**, 703–706.

Cook, K., **Royden, L.**, **Burchfiel, B.**, **Lee, Y.-H.** and **Tan, X.** (2013) Constraints on Cenozoic tectonics in the southwestern Longmen Shan from low-temperature thermochronology. *Lithosphere*, **5**, 393–406.

Cui, B.L. and **Li, X.Y.** (2016) The impact of climate changes on water level of Qinghai Lake in China over the past 50 years. *Hydrol. Res.*, **47**, 532–545.

Dadson, S.J., **Hovius, N.**, **Chen, H.**, **Dade, W.B.**, **Hsieh, M.L.**, **Willett, S.D.**, **Hu, J.-C.**, **Horng, M.-J.**, **Chen, M.-C.**, **Stark, C.P.**, **Lague, D.** and **Lin, J.C.** (2003) Links between erosion, runoff variability and seismicity in the Taiwan orogen. *Nature*, **426**, 648–651.

Das, A., **Krishnaswami, S.** and **Bhattacharya, S.K.** (2005) Carbon isotope ratio of dissolved inorganic carbon (DIC) in rivers draining the Deccan Traps, India: sources of DIC and their magnitudes. *Earth Planet. Sci. Lett.*, **236**, 419–429.

Demurtas, L., **Fontana, D.**, **Lugli, S.** and **Bruno, L.** (2024) Multi-source detrital contributions in the Po alluvial basin (northern Italy) since the Middle Pleistocene. Insights into sediment accumulation in intermediate sinks. *Basin Res.*, **36**, e12858.

Deng, Q.D., **Chen, S.F.** and **Zhao, X.L.** (1994) Tectonics, seismicity and dynamics of Longmenshan Mountains and its adjacent regions. *Seismol. Geol.*, **16**, 389–403.

Deng, K., **Yang, S.**, **von Blanckenburg, F.** and **Wittmann, H.** (2020) Denudation rate changes along a fast-eroding mountainous river with slate headwaters in Taiwan from ^{10}Be (meteoric)/^{9}Be ratios. *J. Geophys. Res. Earth Surf.*, **125**, e2019JF005251.

DiBiase, R.A. and **Whipple, K.X.** (2011) The influence of erosion thresholds and runoff variability on the relationships among topography, climate, and erosion rate. *J. Geophys. Res. Earth Surf.*, **116**, F04036.

Dickinson, W.R. (1970) Relations of andesites, granites, and derivative sandstones to arc-trench tectonics. *Rev. Geophys.*, **8**, 813–860.

Dickinson, W.R. (1985) Interpreting provenance relations from detrital modes of sandstones. In: *Provenance of Arenites* (Ed Zuffa, G.G.), pp. 333–361. Springer, Dordrecht.

Dickinson, W.R. and **Suczek, C.A.** (1979) Plate tectonics and sandstone compositions. *AAPG Bull.*, **63**, 2164–2182.

Dinis, P., **Garzanti, E.**, **Vermeesch, P.** and **Huvi, J.** (2017) Climatic zonation and weathering control on sediment composition (Angola). *Chem. Geol.*, **467**, 110–121.

Dott, R.H., Jr. (2003) The importance of eolian abrasion in supermature quartz sandstones and the paradox of weathering on vegetation-free landscapes. *J. Geol.*, **111**, 387–405.

Drake, L.D. (1970) Rock texture; an important factor for clast shape studies. *J. Sediment. Res.*, **40**, 1356–1361.

Eyankware, M.O., **Ogwah, C.** and **Ike, J.C.** (2021) A synoptic review of mineralogical and chemical characteristics of clays in the southern part of Nigeria. *Res. Ecol.*, **3**, 32–45.

von Eynatten, H., **Tolosana-Delgado, R.** and **Karius, V.** (2012) Sediment generation in modern glacial settings: grain-size and source-rock control on sediment composition. *Sed. Geol.*, **280**, 80–92.

Feng, C., **Zheng, W.**, **Zhang, Y.**, **Shen, X.** and **Wang, W.** (2024) Multiphase tectonic processes in the Mesozoic and formation of early regional geomorphic pattern in the Qilian orogenic belt, northeastern Tibetan Plateau. *Lithosphere*, **2024**, lithosphere_2023_300.

Fu, C.L., **Yan, Z.**, **Guo, X.Q.**, **Niu, M.L.**, **Xia, W.J.**, **Wang, Z.Q.** and **Li, J.L.** (2014) Geochemistry and SHRIMP zircon U-Pb age of diabases in the Lajishankou ophiolitic mélange, South Qilian terrane. *Acta Petrol. Sin.*, **30**, 1695–1706.

Fu, H., **Jian, X.**, **Liang, H.**, **Zhang, W.**, **Shen, X.** and **Wang, L.** (2022) Tectonic and climatic forcing of chemical weathering intensity in the northeastern Tibetan Plateau since the middle Miocene. *Catena*, **208**, 105785.

Fu, H., **Jian, X.**, **Zhang, Z.** and **Pan, H.** (2025) Source-rock, grain-size, weathering, and recycling controls on the feldspar/quartz ratio in silt-sized sediments. *Palaeogeogr. Palaeoclimatol. Palaeoecol.*, **660**, 112700.

Gaillardet, J., **Calmels, D.**, **Romero-Mujalli, G.**, **Zakharova, E.** and **Hartmann, J.** (2019) Global climate control on carbonate weathering intensity. *Chem. Geol.*, **527**, 118762.

Garzanti, E. (2016) From static to dynamic provenance analysis—sedimentary petrology upgraded. *Sed. Geol.*, **336**, 3–13.

Garzanti, E. (2017) The maturity myth in sedimentology and provenance analysis. *J. Sed. Res.*, **87**, 353–365.

Garzanti, E. (2019) Petrographic classification of sand and sandstone. *Earth-Sci. Rev.*, **192**, 545–563.

Garzanti, E. and **Resentini, A.** (2016) Provenance control on chemical indices of weathering (Taiwan river sands). *Sed. Geol.*, **336**, 81–95.

Garzanti, E. and **Vezzoli, G.** (2003) A classification of metamorphic grains in sands based on their composition and grade. *J. Sed. Res.*, **73**, 830–837.

Garzanti, E., **Andò, S.** and **Vezzoli, G.** (2006a) The continental crust as a source of sand (Southern Alps cross section, northern Italy). *J. Geol.*, **114**, 533–554.

Garzanti, E., **Andò, S.**, **Vezzoli, G.**, **Megid, A.A.A.** and **El Kammar, A.** (2006b) Petrology of Nile River sands (Ethiopia and Sudan): sediment budgets and erosion patterns. *Earth Planet. Sci. Lett.*, **252**, 327–341.

Garzanti, E., **Andò, S.** and **Vezzoli, G.** (2008) Settling equivalence of detrital minerals and grain-size dependence of sediment composition. *Earth Planet. Sci. Lett.*, **273**, 138–151.

Garzanti, E., **Limonta, M.**, **Resentini, A.**, **Bandopadhyay, P.C.**, **Najman, Y.**, **Andò, S.** and **Vezzoli, G.** (2013) Sediment recycling at convergent plate margins (Indo-Burman ranges and Andaman–Nicobar Ridge). *Earth-Sci. Rev.*, **123**, 113–132.

Garzanti, E., **Resentini, A.**, **Andò, S.**, **Vezzoli, G.**, **Pereira, A.** and **Vermeesch, P.** (2015) Physical controls on sand composition and relative durability of detrital minerals during ultralong-distance littoral and aeolian transport (Namibia and southern Angola). *Sedimentology*, **62**, 971–996.

Garzanti, E., **Limonta, M.**, **Vezzoli, G.**, **An, W.**, **Wang, J.** and **Hu, X.** (2018) Petrology and multimineral fingerprinting of modern sand generated from a Dissected Magmatic Arc (Lhasa River, Tibet). In: *Tectonics, Sedimentary Basins, and Provenance: A Celebration of the Career of William R. Dickinson* (Eds Ingersoll, R., Lawton, T. and Graham, S.). Geological Society of America Special Paper 540, pp. 197–221. The Geological Society of America, Boulder.

Garzanti, E., **Barbarano, M.**, **Andò, S.**, **Lenzi, M.**, **Deng, K.** and **Yang, S.** (2021a) Provenance of Neogene sandstones in western Taiwan traced with garnet geochemistry and zircon geochronology. *Basin Res.*, **33**, 2069–2088.

Garzanti, E., **Dinis, P.**, **Vezzoli, G.** and **Borromeo, L.** (2021b) Sand and mud generation from continental flood basalts in contrasting landscapes and climatic conditions (Paraná-Etendeka conjugate igneous provinces, Uruguay and Namibia). *Sedimentology*, **68**, 3447–3475.

Garzanti, E., **He, J.**, **Barbarano, M.**, **Resentini, A.**, **Li, C.**, **Yang, L.**, **Yang, S.** and **Wang, H.** (2021c) Provenance versus weathering control on sediment composition in tropical monsoonal climate (South China)-2. Sand petrology and heavy minerals. *Chem. Geol.*, **564**, 119997.

Garzanti, E., **Bayon, G.**, **Dinis, P.**, **Barbarano, M.**, **Pastore, G.**, **Vezzoli, G.**, **Braquet, N.** and **Overare, B.** (2023a) Weathering in the West Africa Craton: mineralogy and geochemistry of Niger River sediments. *J. Geol.*, **131**, 371–409.

Garzanti, E., **Nayak, K.**, **Padoan, M.**, **Vezzoli, G.**, **Resentini, A.**, **Castelltort, S.**, **Lin, A.T.-S.**, **Babonneau, N.**, **Ratzov, G.**, **Hsu, S.-K.** and **Huang, K.F.** (2023b) Fast-eroding Taiwan and transfer of orogenic sediment to forearc basins and trenches in the Philippine and South China seas. *Earth-Sci. Rev.*, **244**, 104523.

Garzanti, E., **Barbarano, M.**, **Dinis, P.**, **Limonta, M.**, **Pastore, G.**, **Vermeesch, P.** and **Vezzoli, G.** (2025) Basaltic sources but quartzose sand: sediment provenance, weathering, and recycling in the Uruguay River catchment. *J. Sed. Res.*, **95**, 675–692.

Gehrels, G.E., **Yin, A.** and **Wang, X.F.** (2003) Detrital-zircon geochronology of the northeastern Tibetan plateau. *Geol. Soc. Am. Bull.*, **115**, 881–896.

Goswami, P.K. and **Deopa, T.** (2018) Petrotectonic setting of the provenance of Lower Siwalik sandstones of the Himalayan foreland basin, southeastern Kumaun Himalaya, India. *Island Arc*, **27**, e12242.

Gu, Z., **Jian, X.**, **Zhai, X.**, **Shen, X.** and **Ye, S.** (2025) Sedimentary records reveal an early Cambrian active margin setting in the NW Yangtze Block, South China. *Palaeogeogr. Palaeoclimatol. Palaeoecol.*, **677**, 113207.

Guan, B.T., **Wang, M.K.**, **Chang, S.H.** and **Wang, H.W.** (2009) Modeling monthly mean temperatures for the mountain regions of Taiwan by generalized additive models. *Agric. For. Meteorol.*, **149**, 281–290.

Guo, R., **Hu, X.**, **Garzanti, E.**, **Lai, W.**, **Yan, B.** and **Mark, C.** (2020) How faithfully do the geochronological and geochemical signatures of detrital zircon, titanite, rutile and monazite record magmatic and metamorphic events? A case study from the Himalaya and Tibet. *Earth-Sci. Rev.*, **201**, 103082.

He, J., **Garzanti, E.**, **Dinis, P.**, **Yang, S.** and **Wang, H.** (2020) Provenance versus weathering control on sediment composition in tropical monsoonal climate (South China)-1. Geochemistry and clay mineralogy. *Chem. Geol.*, **558**, 119860.

He, J., **Garzanti, E.**, **Jiang, T.**, **Barbarano, M.**, **Resentini, A.**, **Liu, E.**, **Chen, S.**, **Shi, G.** and **Wang, H.** (2022) Mineralogy and geochemistry of modern Red River sediments (North Vietnam): provenance and weathering implications. *J. Sed. Res.*, **92**, 1169–1185.

He, J., **Garzanti, E.**, **Jiang, T.**, **Liu, E.**, **Barbarano, M.**, **Resentini, A.** and **Wang, H.** (2025) Sedimentary processes in transport-limited versus weathering-limited erosional regimes: contrasting mineralogical and geochemical signatures of sand and mud in Hainan and Taiwan islands. *Mar. Geol.*, **489**, 107635.

Holloway, N.H. (1982) North Palawan block, Philippines—its relation to Asian mainland and role in evolution of South China Sea. *AAPG Bull.*, **66**, 1355–1383.

Hu, X., **Cao, X.**, **Li, T.**, **Mao, J.**, **Zhang, J.**, **He, X.**, **Zhang, Y.** and **Pan, B.** (2021) Late Quaternary fault slip rate within the Qilian Orogen, insight into the deformation kinematics for the NE Tibetan Plateau. *Tectonics*, **40**, e2020TC006586.

Huang, C.Y., **Yen, Y.**, **Zhao, Q.** and **Lin, C.T.** (2012a) Cenozoic stratigraphy of Taiwan: window into rifting, stratigraphy and paleoceanography of South China Sea. *Chin. Sci. Bull.*, **57**, 3130–3149.

Huang, Q.Y., **Yan, Y.**, **Zhao, Q.H.**, **Liu, P.M.**, **Lin, Y.J.**, **Lin, Q.T.** and **Xie, K.X.** (2012b) Taiwan Cenozoic sequence: reflecting the South China Sea rift, sequence and the mechanism of the paleo ocean change. *Chin. Sci. Bull.*, **57**, 1842–1862.

Jian, X., **Guan, P.**, **Zhang, D.W.**, **Zhang, W.**, **Feng, F.**, **Liu, R.J.** and **Lin, S.D.** (2013) Provenance of Tertiary sandstone in the northern Qaidam basin, northeastern Tibetan Plateau: integration of framework petrography, heavy mineral analysis and mineral chemistry. *Sed. Geol.*, **290**, 109–125.

Jian, X., **Yang, S.**, **Hong, D.**, **Liang, H.**, **Zhang, S.**, **Fu, H.** and **Zhang, W.** (2020a) Seasonal geochemical heterogeneity of sediments from a subtropical mountainous river in SE China. *Mar. Geol.*, **422**, 106120.

Jian, X., **Zhang, W.**, **Yang, S.** and **Kao, S.J.** (2020b) Climate-dependent sediment composition and transport of mountainous rivers in tectonically stable, subtropical East Asia. *Geophys. Res. Lett.*, **47**, e2019GL086150.

Jiang, N.J., **Liu, S.Y.**, **Liu, Y.**, **Wang, X.M.** and **Li, H.J.** (2010) Analysis on flow calculation upper station in Iqe River of Da Qaidam, Qinghai province. *Qinghai Sci. Technol.*, **17**, 64–66.

Jiang, H., **Li, C.**, **Kang, C.**, **Zhang, Y.**, **Wei, C.**, **Zhao, J.** and **Li, Y.** (2020) Provenance discrimination of upper Yangtze River basin sediments: new insights from heavy mineral signatures and detrital magnetite geochemistry. *Quat. Int.*, **568**, 79–89.

Johnsson, M.J. (1993) The system controlling the composition of clastic sediments. In: *Processes Controlling the Composition of Clastic Sediments* (Eds Johnsson, M.J. and Basu, A.). Geol. Soc. Am. Spec. Paper 284 , pp. 1–19. Geological Society of America, Boulder.

Joshi, K.B., **Banerji, U.S.**, **Dubey, C.P.** and **Oliveira, E.P.** (2021) Heavy minerals in provenance studies: an overview. *Arab. J. Geosci.*, **14**, 1330.

Kao, S.J. and **Milliman, J.D.** (2008) Water and sediment discharge from small mountainous rivers, Taiwan: the roles of lithology, episodic events, and human activities. *J. Geol.*, **116**, 431–448.

Kroonenberg, S.B. (1992) Effect of source rock, sorting and postdepositional processes on the bulk geochemistry of fluvial sands in different tectonic and climatic environments. *Geol. Mijnb.*, **71**, 39–50.

Krumbein, W.C. (1941) The effects of abrasion on the size, shape and roundness of lithic fragments. *J. Geol.*, **49**, 482–520.

Lawrence, R.L., **Cox, R.**, **Mapes, R.W.** and **Coleman, D.S.** (2011) Hydrodynamic fractionation of zircon age populations. *Geol. Soc. Am. Bull.*, **123**, 295–305.

Le Pera, E. and **Morrone, C.** (2020) The use of mineral interfaces in sand-sized volcanic rock fragments to infer mechanical durability. *J. Palaeogeogr.*, **9**, 21.

Le Pera, E., **Tangari, A.C.**, **Marinangeli, L.**, **Morrone, C.**, **Riber, L.** and **Andò, S.** (2023) Provenance of modern sands from Baja California rivers (Mexico): petrographic constraints from light and heavy minerals. *J. Sed. Res.*, **93**, 617–641.

Lee, Y.H., **Chen, C.C.**, **Liu, T.K.**, **Ho, H.C.**, **Lu, H.Y.** and **Lo, W.** (2006) Mountain building mechanisms in the Southern Central Range of the Taiwan Orogenic Belt—from accretionary wedge deformation to arc–continental collision. *Earth Planet. Sci. Lett.*, **252**, 413–422.

Li, X.H. (2000) Cretaceous magmatism and lithospheric extension in Southeast China. *J. Asian Earth Sci.*, **18**, 293–305.

Li, J., **Sheng, Y.**, **Chen, J.**, **Wu, J.** and **Wang, S.** (2014) Variations in permafrost temperature and stability of alpine meadows in the source area of the Datong River, Northeastern Qinghai–Tibet Plateau, China. *Permafrost Periglac. Process.*, **25**, 307–319.

Li, B., **Liao, J.**, **Ke, L.**, **Chen, Y.** and **Zhao, X.** (2025) Geological characteristics and prospecting indicators of the Bogong'ao Sn-Cu-Ag polymetallic deposit in Huidong County. *Acta Geologica Sichuan*, **45**, 45–50.

Liang, P. and **Yang, X.** (2023) Grain shape evolution of sand-sized sediments during transport from mountains to dune fields. *J. Geophys. Res. Earth Surf.*, **128**, e2022JF006930.

Liang, W., **Garzanti, E.**, **Hu, X.**, **Resentini, A.**, **Vezzoli, G.** and **Yao, W.** (2022) Tracing erosion patterns in South Tibet: balancing sediment supply to the Yarlung Tsangpo from the Himalaya versus Lhasa Block. *Basin Res.*, **34**, 411–439.

Liang, W., **Hu, X.**, **Garzanti, E.**, **Dong, X.** and **Chen, F.** (2025) Contrasting provenance budgets for suspended load and bedload of the Yarlung Tsangpo, Tibet: Lhasa block or Himalaya? *Geology*, **53**, 333–337.

Liedel, S., **Caracciolo, L.**, **Restrepo, J.C.**, **Weltje, G.J.**, **Lucà, F.**, **Beltrán-Triviño, A.** and **Restrepo Ángel, J.D.** (2024) A quantitative provenance analysis (QPA) approach to quantify controls on sediment generation and sediment flux in the upper reaches of the Magdalena River (Colombia): 1. Natural and anthropic controls on the sand fraction. *J. Geophys. Res. Earth Surf.*, **129**, e2023JF007369.

Liu, Z., **Si, J.**, **Deng, Y.**, **Jia, B.**, **Li, X.**, **He, X.**, **Zhou, D.**, **Wang, C.**, **Zhu, X.**, **Qin, J.**, **Ndayambaza, B.** and **Wang, B.** (2023) Assessment of land desertification and its drivers in semi-arid alpine mountains: a case study of the Qilian Mountains Region, Northwest China. *Remote Sens.*, **15**, 3836.

Liu, C., **Zhang, Y.**, **Lu, C.**, **Wang, X.** and **Li, H.** (2024) Spatio-temporal evolution and causes of land subsidence in the Jiulong River Estuary region based on time-series InSAR. *J. Appl. Oceanogr.*, **43**, 116–125.

Lou, J.Y., **Chen, C.T.A.**, **Lui, H.K.**, **Selvaraj, K.**, **Zhang, S.R.** and **Lu, X.X.** (2014) Comparison of subtropical surface water chemistry between the large Pearl River in China and small mountainous rivers in Taiwan. *J. Asian Earth Sci.*, **79**, 182–190.

Ma, Y.J., **Li, X.Y.**, **Liu, L.**, **Huang, Y.M.**, **Li, Z.**, **Hu, X.**, **Wu, X.-C.**, **Yang, X.-F.**, **Wang, P.**, **Zhao, S.-J.**, **Zhang, G.-H.** and **Liu, B.Y.** (2018) Measurements and modeling of the water budget in semiarid high-altitude Qinghai Lake Basin, Northeast Qinghai-Tibet plateau. *J. Geophys. Res. Atmos.*, **123**, 10–857.

Marques, E.A.G., **Williams, D.J.**, **Assis, I.R.** and **Leão, M.F.** (2017) Effects of weathering on characteristics of rocks in a subtropical climate: weathering morphology, in situ, laboratory and mineralogical characterization. *Environ. Earth Sci.*, **76**, 602.

Mazumder, R. (2017) Sediment provenance: influence on compositional change from source to sink. In: *Sediment Provenance* (Ed Mazumder, R.), pp. 1–4. Elsevier, Amsterdam, The Netherlands.

Mo, L., **Yu, X.**, **Feng, Y.** and **Jiang, T.** (2025) Runoff variations and quantitative analysis in the Qinghai Lake Basin under changing environments. *Hydrology*, **12**, 94.

Montgomery, D.R. and **Brandon, M.T.** (2002) Topographic controls on erosion rates in tectonically active mountain ranges. *Earth Planet. Sci. Lett.*, **201**, 481–489.

Moon, S., **Huh, Y.**, **Qin, J.** and **van Pho, N.** (2007) Chemical weathering in the Hong (Red) River basin: rates of silicate weathering and their controlling factors. *Geochim. Cosmochim. Acta*, **71**, 1411–1430.

Moosdorf, N., **Cohen, S.** and **von Hagke, C.** (2018) A global erodibility index to represent sediment production potential of different rock types. *Appl. Geogr.*, **101**, 36–44.

Nesbitt, H.W. and **Young, G.M.** (1996) Petrogenesis of sediments in the absence of chemical weathering: effects of abrasion and sorting on bulk composition and mineralogy. *Sedimentology*, **43**, 341–358.

New, M., **Lister, D.**, **Hulme, M.** and **Makin, I.** (2002) A high-resolution data set of surface climate over global land areas. *Clim. Res.*, **21**, 1–25.

Nie, J., **Stevens, T.**, **Rittner, M.**, **Stockli, D.**, **Garzanti, E.**, **Limonta, M.**, **Bird, A.**, **Andò, S.**, **Vermeesch, P.**, **Saylor, J.**, **Lu, H.**, **Breecker, D.**, **Hu, X.**, **Liu, S.**, **Resentini, A.**, **Vezzoli, G.**, **Peng, W.**, **Carter, A.**, **Ji, S.** and **Pan, B.** (2015) Loess plateau storage of northeastern Tibetan plateau-derived Yellow River sediment. *Nat. Commun.*, **6**, 8511.

Ott, R., **Gallen, S.F.** and **Helman, D.** (2023) Erosion and weathering in carbonate regions reveal climatic and tectonic drivers of carbonate landscape evolution. *Earth Surf. Dyn.*, **11**, 247–257.

Oumar, K.O., **Gilbert François, N.N.**, **Bertrand, M.M.**, **Nathanael, T.**, **Constantin, B.E.**, **Simon, M.J.** and **Jacques, E.** (2022) Mineralogical, geochemical characterization and physicochemical properties of kaolinitic clays of the Eastern Part of the Douala Sub-Basin, Cameroon, Central Africa. *Appl. Sci.*, **12**, 9143.

Palomares, M. and **Arribas, J.** (1993) Modern stream sands from compound crystalline sources: composition and sand generation index. In: *Processes Controlling the Composition of Clastic Sediments* (Eds Johnsson, M.J. and Basu, A.). Geol. Soc. Am. Spec. Paper 284 , pp. 313–322. Geological Society of America, Boulder.

Peng, S. (2019) *1-Km Monthly Mean Temperature Dataset for China (1901–2021)*. National Tibetan Plateau/Third Pole Environment Data Center, Beijing.

Peng, S. (2020) *1-Km Monthly Precipitation Dataset for China (1901–2021)*. National Tibetan Plateau/Third Pole Environment Data Center, Beijing.

Picard, M.D. and **McBride, E.F.** (2007) Comparison of river and beach sand composition with source rocks, Dolomite Alps drainage basins, northeastern Italy. In: *Sedimentary Provenance and Petrogenesis: Perspectives from Petrography and Geochemistry* (Eds Arribas, J., Johnsson, M.J. and Critelli, S.), *Geological Society of America Special Paper*, 420, pp. 1–12. Geological Society of America.

Potter, P.E., **Huh, Y.** and **Edmond, J.M.** (2001) Deep-freeze petrology of Lena River sand, Siberia. *Geology*, **29**, 999–1002.

Powell, C.M.A. (1979) A morphological classification of rock cleavage. *Tectonophysics*, **58**, 21–34.

Resentini, A., **Goren, L.**, **Castelltort, S.** and **Garzanti, E.** (2017) Partitioning sediment flux by provenance and tracing erosion patterns in Taiwan. *J. Geophys. Res. Earth Surf.*, **122**, 1430–1454.

Resentini, A., **Andò, S.** and **Garzanti, E.** (2018) Quantifying roundness of detrital minerals by image analysis: sediment transport, shape effects, and provenance implications. *J. Sed. Res.*, **88**, 276–289.

Rohrmann, A., **Heermance, R.**, **Kapp, P.** and **Cai, F.** (2013) Wind as the primary driver of erosion in the Qaidam Basin, China. *Earth Planet. Sci. Lett.*, **374**, 1–10.

Saha, S., **Reza, A.H.M.S.** and **Roy, M.K.** (2020) Illite crystallinity index an indicator of physical weathering of the Sediments of the Tista River, Rangpur, Bangladesh. *Int. J. Adv. Geosci.*, **8**, 27–32.

Schneider, S., **Hornung, J.**, **Hinderer, M.** and **Garzanti, E.** (2016) Petrography and geochemistry of modern river sediments in an equatorial environment (Rwenzori Mountains and Albertine rift, Uganda)—implications for weathering and provenance. *Sed. Geol.*, **336**, 106–119.

Searle, M.P. (2001) Conference report: 15th Himalaya–Karakoram–Tibet Workshop, Chengdu, China, 21–24 April 2000. *J. Asian Earth Sci.*, **19**, 547–551.

Shen, X., **Jian, X.**, **Li, C.**, **Liu, J.T.**, **Chang, Y.P.**, **Zhang, S.**, **Mei, H.**, **Fu, H.** and **Zhang, W.** (2021) Submarine topography-related spatial variability of the southern Taiwan Strait sands (East Asia). *Mar. Geol.*, **436**, 106495.

Shen, X., **Jian, X.**, **Zhang, W.** and **Guan, P.** (2024) Grain textural bias in detrital single-mineral provenance studies. *Sed. Geol.*, **471**, 106731.

Shen, X., **Jian, X.**, **Zhang, W.**, **Ye, S.**, **Liang, H.**, **Zhuang, Y.** and **Guan, P.** (2025) Cenozoic sandstone provenance in the Qaidam Basin of China, and its implications for the deformation history of the Tibetan Plateau. *Palaeogeogr. Palaeoclimatol. Palaeoecol.*, **675**, 113120.

Singh, S.K., **Kumar, A.** and **France-Lanord, C.** (2006) Sr and $^{87}Sr/^{86}Sr$ in waters and sediments of the Brahmaputra river system: silicate weathering, CO_2 consumption and Sr flux. *Chem. Geol.*, **234**, 308–320.

Singh, M., **Singh, I.B.** and **Müller, G.** (2007) Sediment characteristics and transportation dynamics of the Ganga River. *Geomorphology*, **86**, 144–175.

Su, N., **Yang, S.**, **Guo, Y.**, **Yue, W.**, **Wang, X.**, **Yin, P.** and **Huang, X.** (2017) Revisit of rare earth element fractionation during chemical weathering and river sediment transport. *Geochem. Geophys. Geosyst.*, **18**, 935–955.

Sun, H., **Zhong, D.** and **Zhan, W.** (2019) Reservoir characteristics in the Cretaceous volcanic rocks of Songliao Basin, China: a case of dynamics and evolution of the volcano-porosity and diagenesis. *Energy Explor. Exploitation*, **37**, 607–625.

Sun, H.Y., **Ma, F.**, **Wang, G.L.**, **Zhu, X.**, **Zhang, W.** and **Chen, L.M.** (2025) Geothermal reservoir forming model in Fujian Province I: fluid geochemical characteristics and formation mechanism. *Earth Sci.*, **50**, 3241–3269.

Tang, M. (1985) The distribution of precipitation in Mountain Qilian (Nanshan). *Acta Geogr. Sin.*, **40**, 323–332.

Tang, J. (2022) Discussion on the stratigraphic characteristics and diachroneity of the Fotan Formation along the coastal area of Fujian. *Geol. Fujian*, **41**, 126–136.

Tian, Y., **Kohn, B.P.**, **Gleadow, A.J.W.** and **Hu, S.** (2013) Constructing the Longmen Shan eastern Tibetan Plateau margin: insights from low-temperature thermochronology. *Tectonics*, **32**, 576–592.

Tung, K.A., **Yang, H.Y.**, **Liu, D.Y.**, **Zhang, J.X.**, **Yang, H.J.** and **Sha, Y.H.** (2013) The Neoproterozoic granitoids from the Qilian Block, NW China: evidence for a link between the Qilian and South China blocks. *Precambrian Res.*, **235**, 163–189.

Van de Kamp, P.C. (2010) Arkose, subarkose, quartz sand, and associated muds derived from felsic plutonic rocks in glacial to tropical humid climates. *J. Sed. Res.*, **80**, 895–918.

Vezzoli, G., **Garzanti, E.**, **Limonta, M.**, **Andò, S.** and **Yang, S.** (2016) Erosion patterns in the Changjiang (Yangtze River) catchment revealed by bulk-sample versus single-mineral provenance budgets. *Geomorphology*, **261**, 177–192.

Wadell, H. (1932) Volume, shape, and roundness of rock particles. *J. Geol.*, **40**, 443–451.

Wang, L.B., **Li, J.**, **Zhao, J.T.** and **Zhai, B.** (2013) Detrital minerals in the surrounding river sediments, Liaodong Bay, Bohai Sea: composition and its geological significance. *Acta Sedimentol. Sin.*, **31**, 663–671.

Wang, Z.B., **Li, R.H.**, **Yang, S.Y.**, **Bai, F.L.**, **Mei, X.**, **Zhang, J.** and **Lu, K.** (2019) Comparison of detrital mineral compositions between stream sediments of the Yangtze River (Changjiang) and the Yellow River (Huanghe) and their provenance implication. *China Geol.*, **2**, 169–178.

Wang, W., **Godard, V.**, **Liu-Zeng, J.**, **Zhang, J.**, **Li, Z.**, **Xu, S.**, **Yao, W.**, **Yuan, Z.**, **Aumaître, G.**, **Bourlès, D.L.** and **Keddadouche, K.** (2021a) Tectonic controls on surface erosion rates in the Longmen Shan, Eastern Tibet. *Tectonics*, **40**, e2020TC006445.

Wang, Z., **Li, X.** and **Hou, X.** (2021b) Hydrogeochemistry of river water in the upper reaches of the Datong River Basin, China: implications of anthropogenic inputs and chemical weathering. *Acta Geol. Sinica*, **95**, 962–975.

Wang, J., **Wang, Z.**, **Cheng, H.**, **Kang, J.** and **Liu, X.** (2022) Land cover changing pattern in pre- and post-earthquake affected area from remote sensing data: a case of Lushan County, Sichuan Province. *Land*, **11**, 1205.

Wang, L., **Jian, X.**, **Mei, H.**, **Shen, X.** and **Fu, H.** (2024) Clay composition heterogeneity in sediments from mountainous catchments with contrasting bedrock lithology in SE China coast. *Catena*, **247**, 108470.

Wang, S., **Li, C.**, **Duan, Z.**, **Ng, N.C.W.** and **Yang, S.** (2025) Climate and topography controls on chemical weathering in Changjiang River Basin. *Glob. Planet. Change*, **251**, 104841.

Wei, C.J., **Yang, Y.**, **Su, X.L.**, **Song, S.G.** and **Zhang, L.F.** (2009) Metamorphic evolution of low-T eclogite from the North Qilian orogen, NW China: evidence from petrology and calculated phase equilibria in the system NCKFMASHO. *J. Metamorph. Geol.*, **27**, 55–70.

Weltje, G.J. (2006) Ternary sandstone composition and provenance: an evaluation of the 'Dickinson model'. *Geol. Soc. Lond. Spec. Publ.*, **264**, 79–99.

Wu, L., **Liu, C.**, **Liu, W.** and **Zhang, H.** (2021) Detrital zircon U–Pb geochronology and provenance of Triassic sandstones from the Qilian Mountains, northeastern margin of the Tibetan Plateau. *Geoscience*, **35**, 1178–1193.

Wu, K., **Tan, X.**, **Liu, X.**, **Pang, P.**, **Wu, S.**, **Xue, S.**, **Xing, H.**, **Xiong, Y.**, **Li, Y.**, **Zhang, M.**, **Deng, W.** and **Wang, J.** (2024) High-frequency lacustrine lithological and geochemical variations in the Eocene Qaidam Basin: implications for paleoenvironment reconstruction. *Minerals*, **14**, 79.

Xiang, D. (1982) The characteristics of geological structures in the Qilianshan region, China. *Sci. Geol. Sin.*, **17**, 364–370.

Xu, Z., **Liu, L.**, **Zheng, H.**, **Ji, J.**, **Chen, J.**, **Teng, H.H.** and **Li, G.** (2025) Control of temperature on the weathering of slow-eroding post-orogenic terrains. *Glob. Planet. Change*, **252**, 104901.

Yang, S., **Jung, H.-S.** and **Li, C.** (2004) Two unique weathering regimes in the Changjiang and Huanghe drainage basins: geochemical evidence from river sediments. *Sed. Geol.*, **164**, 19–34.

Yang, L., **Song, S.**, **Su, L.**, **Allen, M.B.**, **Niu, Y.**, **Zhang, G.** and **Zhang, Y.** (2019) Heterogeneous oceanic arc volcanic rocks in the South Qilian Accretionary Belt (Qilian Orogen, NW China). *J. Petrol.*, **60**, 85–116.

Yao, T.D., **Thompson, L.G.**, **Mosbrugger, V.**, **Zhang, F.**, **Ma, Y.M.**, **Luo, T.X.**, **Xu, B.**, **Yang, X.**, **Joswiak, D.R.**, **Wang, W.**, **Joswiak, M.E.**, **Devkota, L.P.**, **Tayal, S.**, **Jilani, R.** and **Grigholm, B.** (2012) Third pole environment (TPE). *Environ. Dev.*, **3**, 52–64.

Yao, T.D., **Masson-Delmotte, V.**, **Gao, J.**, **Yu, W.S.**, **Yang, X.X.**, **Risi, C.**, **Sturm, C.**, **Werner, M.**, **Zhao, H.**, **He, Y.**, **Ren, W.**, **Tian, L.**, **Shi, C.** and **Ren, W.** (2013) A review of climatic controls on δ18O in precipitation over the Tibetan Plateau: observations and simulations. *Rev. Geophys.*, **51**, 525–548.

Ye, S., **Jian, X.**, **Fu, L.**, **Zhang, W.**, **Shen, X.** and **Guan, P.** (2024) Detrital muscovite 40Ar/39Ar geochronology and provenance of Cenozoic deposits in the Qaidam basin, northern Tibetan Plateau and comparison with detrital zircon and apatite records. *Mar. Petrol. Geol.*, **169**, 107068.

Yu, X., **Fu, S.**, **Wang, Z.**, **Li, Q.** and **Guo, Z.** (2017) The discovery of early Paleoproterozoic high-Na trondhjemite in the northeastern Qaidam basin: evidence from the drilling core samples. *Precambrian Res.*, **298**, 615–628.

Zeroual, A., **Assani, A.A.**, **Meddi, M.** and **Alkama, R.** (2019) Assessment of climate change in Algeria from 1951 to 2098 using the Köppen–Geiger climate classification scheme. *Clim. Dyn.*, **52**, 227–243.

Zhang, T.T. (2024) Treatment measures for engineering geological problems of the dam foundation of Xiangxi Reservoir in Nanjing County. *Water Conservancy Sci. Technol.*, **4**, 29–32.

Zhang, Y., **Li, Y.**, **Zhou, R.J.**, **Densmore, A.L.** and **Richardson, N.J.** (2006) Denudation process in the eastern margin of the Qinghai–Tibet Plateau since the Late Cenozoic: evidence from fission track dating. *Sed. Geol. Tethyan Geol.*, **26**, 97–102.

Zhang, X., **Chen, H.** and **Lin, X.F.** (2009) Changes of climatic features in the Minjiang River Basin in recent 45 years. *Res. Soil Water Conserv.*, **16**, 107–110.

Zhang, H.-P., **Zhang, P.-Z.**, **Kirby, E.**, **Yin, J.-H.**, **Liu, C.-R.** and **Yu, G.-H.** (2011) Along-strike topographic variation of the Longmen Shan and its significance for landscape evolution along the eastern Tibetan Plateau. *J. Asian Earth Sci.*, **40**, 855–864.

Zhang, J.Y., **Yin, A.**, **Liu, W.C.**, **Wu, F.Y.**, **Lin, D.** and **Grove, M.** (2012) Coupled U-Pb dating and Hf isotopic analysis of detrital zircon of modern river sand from the Yalu River (Yarlung Tsangpo) drainage system in southern Tibet: constraints on the transport processes and evolution of Himalayan rivers. *GSA Bull.*, **124**, 1449–1473.

Zhang, X., **Lin, C.M.**, **Dalrymple, R.W.** and **Yang, S.Y.** (2021) Source-to-sink analysis for the mud and sand in the late-Quaternary Qiantang River incised-valley fill and its implications for delta-shelf–estuary dispersal systems globally. *Sedimentology*, **68**, 3228–3252.

Zhang, S., **Jian, X.**, **Liu, J.T.**, **Wang, P.**, **Chang, Y.P.** and **Zhang, W.** (2022) Climate-driven drainage reorganization of small mountainous rivers in Taiwan (East Asia) since the last glaciation: the Zhuoshui River example. *Palaeogeogr. Palaeoclimatol. Palaeoecol.*, **586**, 110759.

Zhao, X.L., **Deng, Q.D.** and **Chen, S.F.** (1994a) Tectonic geomorphology of the central segment of the Longmenshan Thrust Belt, west Sichuan, Southwestern China. *Seismol. Geol.*, **16**, 422–428.

Zhao, X.L., **Deng, Q.D.** and **Chen, S.F.** (1994b) Tectonic geomorphology of the Minshan Uplift in the western Sichuan, Southwestern China. *Seismol. Geol.*, **16**, 429–439.

Zhao, Y., **Yang, S.**, **Liu, J.T.**, **Fan, D.**, **Yang, R.J.** and **Bi, L.** (2017) Reconstruction of silicate weathering intensity and paleoenvironmental change during the late Quaternary in the Zhuoshui River catchment in Taiwan. *Quat. Int.*, **452**, 43–53.

Zhou, Y.W., **Guo, D.X.**, **Qiu, G.Q.**, **Cheng, G.D.** and **Li, S.D.** (2000) *Geocryology in China*. Science Press, Beijing.

Zoleikhaei, Y., **Mulder, J.A.** and **Cawood, P.A.** (2022) Evaluating sediment recycling through combining inherited petrogenic and acquired sedimentary features of multiple detrital minerals. *Basin Res.*, **34**, 1055–1083.

Zuza, A.V., **Cheng, X.** and **Yin, A.** (2016) Testing models of Tibetan Plateau formation with Cenozoic shortening estimates across the Qilian Shan-Nan Shan thrust belt. *Geosphere*, **12**, 501–532.

Manuscript received 5 March 2026; revision accepted 9 July 2026

Supporting Information

Additional information may be found in the online version of this article:

Table S1. Petrographic composition data of all samples from our study area.

Table S2. Published petrographic composition data compiled in this study.

Table S3. References for the published petrographic composition data compiled in this study.

Table S4. Quartz roundness data for the analysed samples.

Table S5. Lithic fragment roundness data of analysed samples.

Table S6. Lithic fragment aspect ratio data of analysed samples.

Fig. S1. Representative photomicrographs of analysed river sand samples showing variations in carbonate lithic fragment abundance.

Fig. S2. Representative photomicrographs of analysed river sand samples grouped by inferred sedimentary recycling cycles.

Fig. S3. Representative photomicrographs of analysed river sand samples from small, lithologically homogeneous rivers.

Fig. S4. Representative photomicrographs of analysed river sand samples showing lithic fragments with distinct morphologies.

Fig. S5. Detrital zircon U–Pb age spectra of rivers sand samples, grouped by inferred sedimentary recycling cycles.